Mon. Not. R. Astron. Soc. **000**, 1–19 (2007) Printed 19 February 2007 (MN LATEX style file v2.2)

Highly ionised plasma in the Large Magellanic Cloud: Evidence for outflows and a possible galactic wind⋆

N. Lehner & J.C. Howk
Department of Physics, University of Notre Dame, 225 Nieuwland Science Hall, Notre Dame, IN 46556, USA

Accepted XXX. Received XXX.

ABSTRACT

Based on an analysis of the interstellar highly ionised species C IV, Si IV, N V, and O VI observed in the *FUSE* and *HST*/STIS E140M spectra of four hot stars in the Large Magellanic Cloud (LMC), we find evidence for a hot LMC halo fed by energetic outflows from the LMC disk and even possibly an LMC galactic wind. Signatures for such outflows are the intermediate and high-velocity components ($v_{\rm LSR} \gtrsim 100\,{\rm km\,s^{-1}}$) relative to the LMC disk observed in the high- and low-ion absorption profiles. The stellar environments produce strong, narrow ($T \lesssim 2 \times 10^4$ K) components of C IV and Si IV associated with the LMC disk; in particular they are likely signatures of H II regions and expanding shells. Broad components are observed in the profiles of C IV, Si IV, and O VI with their widths implying hot, collisionally ionised gas at temperatures of a few times 10^5 K. There is a striking similarity in the O VI/C IV ratios for the broad LMC and high-velocity components, suggesting much of the material at $v_{\rm LSR} \gtrsim 100\,{\rm km\,s^{-1}}$ is associated with the LMC. The velocity of the high-velocity component is large enough to escape altogether the LMC, polluting the intergalactic space between the LMC and the Milky Way. The observed high-ion ratios of the broad LMC and high-velocity components are consistent with those produced in conductive interfaces; such models are also favored by the apparent kinematically coupling between the high and the weakly ionised species.

Key words: ISM: clouds – ISM: kinematics and dynamics – ISM: structure – galaxies: ISM – galaxies: individual: Large Magellanic Cloud – ultraviolet: ISM

1 INTRODUCTION

The structure and energetics of the interstellar medium (ISM) in galaxies are strongly influenced by stellar winds and supernovae (e.g., Abbott 1982). This is particularly true for spiral and irregular galaxies with on-going massive star formation, such as the Milky Way, and the Large and Small Magellanic Clouds (LMC, SMC). The input of energy from winds and supernovae is expected to affect the ISM on kiloparsec scales, creating regions of super-heated gas (e.g., Norman & Ikeuchi 1989). The 10^6 K gas that expands into the halo of a disk galaxy may eventually cool and fall back onto the disk in a massive system, participating in a galactic fountain (Shapiro & Field 1976); in a low mass system, this material may escape the galaxy altogether in a galactic wind (Breitschwerdt, Voelk, & McKenzie 1991). Galactic fountains and winds affect the scale over which newly produced metals are distributed in the ISM of a galaxy and/or in the intergalactic medium. For example, outflows can affect the [α/Fe] ratios inside and outside dwarf galaxies (Recchi, Matteucci, & D'Ercole 2001). Gas dynamics are therefore critical in determining the evolution of galaxies (e.g., Matteucci 2003). Characterising the phenomena of infall and outflow in nearby galaxies is crucial for understanding the role they may play in galaxy evolution and in the enrichment and evolution of the intergalactic medium.

The LMC is the nearest gas-rich disk galaxy to our own Milky Way. As such it has been the target of intense studies of its interstellar medium (ISM), including its dust (e.g., Meixner et al. 2006), its molecular gas (Tumlinson et al. 2002), its warm H I (Kim et al. 2003), its warm ionised gas traced by Hα emission (e.g., Danforth et al. 2002), its warm-hot gas traced by O VI (Howk et al. 2002; Danforth & Blair 2006), and its hot gas traced by X-rays (e.g., Snowden & Petre 1994). In this work, we report observations of interstellar absorption from the Li-like ions N V, C IV, Si IV, and O VI towards stars within the LMC. These ions give us the means to study the highly-ionised material produced by feedback processes in the Milky Way and in the Magellanic Clouds. Si IV, C IV, N V, and O VI peak in abundance at (0.6,1.0,1.8, and 2.8) $\times 10^5$ K, respectively, in collisional ionisation equilibrium

⋆ Based on observations made with the NASA-CNES-CSA Far Ultraviolet Spectroscopic Explorer. FUSE is operated for NASA by the Johns Hopkins University under NASA contract NAS5-32985. Based on observations made with the NASA/ESA Hubble Space Telescope, obtained at the Space Telescope Science Institute, which is operated by the Association of Universities for Research in Astronomy, Inc. under NASA contract No. NAS5-26555.

(CIE; Sutherland& Dopita 1993). They are, however, unlikely to be in equilibrium since these temperatures correspond to the peak of the interstellar cooling curve, and gas at those temperatures is likely to cool faster than it recombines. Instead, these ions may trace interfaces between very hot gas ($T \gtrsim 10^6$ K) and warm or cool ($T \lesssim 10^4$ K) material and serve as a probe of the interaction between the phases of the ISM having the most mass (warm/cool gas) and the most direct connection to feedback processes (hot gas).

Observational searches for a hot corona about the LMC using the highly ionised species started with *IUE* spectra of C IV, Si IV, and N V towards the hot star Sk$-67^\circ 104$ (de Boer & Savage 1980). However, the crude spectral resolution of *IUE* and the fact that that the hot star could be partly responsible for producing C IV and Si IV brought Chu et al. (1994) to conclude these observations were not sufficient to prove the existence of a hot LMC halo (N V was only marginally detected at best). These highly ionised species could be either produced by photoionisation from the star itself or in the superbubble via shocks. Wakker et al. (1998) found C IV absorption in the spectra of cooler stars (O9.7–B1) using modest resolution *HST* spectroscopy. This was the first evidence of C IV not related directly to local effects, as these stars were deemed unable to produce significant high-ion absorption via photoionisation.

More recently, *FUSE* has contributed to the effort of examining the hot gas in the LMC by probing diffuse O VI in both Magellanic Clouds (Howk et al. 2002; Hoopes et al. 2002; Danforth et al. 2002; Danforth & Blair 2006). Howk et al. (2002) used *FUSE* observations of sight lines to the LMC to study the O VI content and kinematics of the LMC. Their survey of 12 sight lines through the near side of the LMC probed collisionally-ionised gas at $T \sim 3\times10^5$ K in the LMC and shows in particular that the LMC contains a significant amount of highly-ionised gas, with O VI column densities equal or greater than those found along extended paths through the Milky Way; and much of the O VI in the LMC must reside in an extended "halo" or thick disk distribution, likely similar to that found in our Galaxy (Savage et al. 2003).

These studies of the individual highly ionised species have broadly sketched a picture of the hot gas in the LMC and the presence of coronal hot gas, but a crucial step is to combine all the available highly ionised species observed with *HST*/STIS E140M and *FUSE* for a better understanding of the highly ionised gas in the LMC. In this paper, we take such a step by presenting the detailed kinematics and high-ion absorption (O VI, C IV, Si IV, and N V) towards four stars in the LMC using *FUSE* and STIS. Two of these sight lines probe prominent superbubbles, while the other two probe H II regions, allowing us to compare the highly ionised species and their connection with weaker ions towards different types of interstellar regions, which is useful for differentiating local from global effects. The organisation of this paper is as follows. After describing the observations, data reduction, and analysis of the data (measurements of the kinematics, column densities, and column density ratios) in §2, we present an overview of the kinematics in §3. In §4 we discuss the origin of the highly ionised plasma in the LMC and the implications of our results. A summary of the main results is presented in §5.

2 OBSERVATIONS AND ANALYSIS

2.1 Database

From the data archives of *FUSE* and *HST*/STIS E140M, we selected four LMC targets. The selection criteria were to have the four critical highly ionised species (Si IV, C IV, N V, and O VI) observable in the FUV and UV and to be able to model these ions without too much uncertainties (i.e. with a continuum near the relevant ions that can be modeled without too much uncertainty). This resulted in the sample of the four stars presented in Table 1. Fortuitously, these stars are also located in different interstellar environments (from Chu et al. 1994 and references therein):
(1) Sk$-65^\circ 22$ is projected within the supergiant shell LMC 1, which is about 1 kpc across (Meaburn 1980). It is located in a faint H II region DEM 48 at the southeast rim. This supergiant shell contains the OB association LH 15.
(2) Sk$-67^\circ 211$ is in the H II region DEM 241 that contains the OB association LH 82. The bright UV continuum and the early spectral type (O2 III(f*), Walborn et al. 2002) imply the star can likely produce strong C IV and Si IV absorption associated with its stellar environment.
(3) Sk$-69^\circ 246$ is a WR star situated in the X-ray bright superbubble 30 Dor, and more precisely is in the south end of Shell 5, which is the X-ray-bright "chimney" to the north of the LH 100 OB association (Y.-H. Chu 2006, priv. comm.).
(4) Sk$-71^\circ 45$ is located in the superbubble DEM 221 associated with the OB association LH 69.

2.2 The *FUSE* observations

The *FUSE* observations are from the PI team programs P103 (PI: Sembach) and P117 (PI: Hutchings). Descriptions of the *FUSE* instrument design and inflight performance are found in Moos et al. (2000) and Sahnow et al. (2000). The LiF 1A, LiF 2B, SiC 1A, and SiC 2B segment spectra cover the wavelength region of the O VI $\lambda\lambda$1031.926, 1037.617 doublet. However, we have chosen not to use the SiC 2B data because of the strong fixed pattern noise and relatively low resolution of observations near O VI when using this segment. Observations in the SiC 1A and LiF 2B segments have $\sim$30% and $\sim$60% of the sensitivity of the LiF 1A segment, respectively. Therefore, we principally use the LiF 1A segment for our measurements. We did not find any difference between the O VI profiles observed in the different segments (within the signal-to-noise). We did not combine the measurements from the three different segments to maintain the optimal spectral resolution. The observations were obtained in the LWRS ($30''\times30''$) apertures. We use the current calibration pipeline software (CALFUSE version 3.0.8 and higher) to extract and calibrate the observations.

The zero point in the final wavelength scale was established by first estimating an average *FUSE* velocity using the ISM lines of Si II λ1020.699, Ar I λ1066.660, Fe II λ1055.262. We used these lines because (i) they are not too saturated to be able to measure the centroids accurately; (ii) they are present in the LiF 1A segment and encompass the O VI λ1031.926 interstellar absorption line, minimising spurious wavelength shifts; (iii) they trace the same gas that the ions used in the STIS wavelength range (S II, Fe II, and Ni II). We then shift the *FUSE* wavelength to the absolute LSR frame determined with the accurate STIS spectra. We estimate that the relative *FUSE* velocity calibration of the O VI is accurate to $\sim$5 $\mathrm{km\,s^{-1}}$ after comparing the shifts needed for the velocity centroids C II, Fe II, Si II in *FUSE* to match the LSR velocity of similar ions in STIS E140M.

2.3 The STIS E140M observations

The STIS E140M Observations were obtained through the GO program 8662 in Cycle 9 (PI: J. Lauroesch). This program was built

Table 1. Summary of stellar and sightline properties

Name	Alias	Type	l (°)	b (°)	V (mag)	v_∞ ($\mathrm{km\,s^{-1}}$)	$v(\mathrm{H}\alpha)$ ($\mathrm{km\,s^{-1}}$)	Environments[a]
Sk−65°22	HD 270952	O6 Iaf+	276.40	–35.75	12.07	1337	270 ± 15	Supergiant shell DEM 48 (N 13)
Sk−67°211	HD 269810	O2 III(f*)	277.70	–32.16	12.28	3593	285 ± 17	H II region DEM 241 (N 59A)
Sk−69°246	HD 38282	WN6h	279.38	–31.66	11.15	1835	252	X-ray bright superbubble 30 Dor
Sk−71°45	HD 269676	O4–5 III(f)	281.86	–32.02	11.51	2488	227 ± 19	Superbubble DEM 221 (N 206)

Note: Spectral types and terminal velocities are from Walborn et al. (2002) and Massa et al. (2003) for Sk−65°22, Sk−67°211, and Sk−71°45 and from Willis et al. (2004) for Sk−69°246. $v(\mathrm{H}\alpha)$ are from Danforth (2003), except towards Sk−69°246 where it comes from Chu et al. (1994) and references therein. Velocities are in the LSR frame. a : from Chu et al. (1994). The designations DEM and N refer to entry in the catalog of Davies, Elliott, & Meaburn (1976) and Henize (1956), respectively.

as a snapshot survey to complement the *FUSE* O VI observations by providing coverage of the other highly ionised species, C IV, N V, and Si IV. The STIS data were obtained with the E140M intermediate-resolution echelle grating. The entrance slit was set to $0\farcs2 \times 0\farcs2$. The spectral resolution is 7 $\mathrm{km\,s^{-1}}$ with a detector pixel size of 3.5 $\mathrm{km\,s^{-1}}$. Information about STIS and its in-flight performance is given by Woodgate et al. (1998), Kimble et al. (1998), and in the STIS Instrument Handbook (Proffitt et al. 2002).

Standard calibration and extraction procedures were employed using the CALSTIS routine (version 2.2). The STIS data reductions provide an excellent wavelength calibration with a velocity uncertainty of $\sim$1 $\mathrm{km\,s^{-1}}$. The heliocentric velocity was corrected to the dynamical local standard of rest-frame (LSR) (Mihalas & Binney 1981).

2.4 Selection of species and velocity structures

The main goal of this work is to study the properties and origin(s) of the highly ionised species in the LMC. O VI λ1031.926, N V $\lambda\lambda$1238.821,1242.804, C IV $\lambda\lambda$1548.195,1550.770, and Si IV $\lambda\lambda$1393.755,1402.770 are the highly ionised species at hand. The excitation potentials are 113.9 eV, 77.5 eV, 47.9 eV, and 33.5 eV for O VI, N V, C IV, and Si IV, respectively. Therefore, O VI and N V are better diagnostics of shock-heated gas than C IV and Si IV, the latter being susceptible to photoionisation.

To understand the connection, if any, between the highly ionised species and the weakly ionised species, we have to investigate the kinematics of the ions tracing cool/warm and hot gas. For tracing the cool/warm gas we use the low-ionisation species O I λ1302.169 Si II λ1526.707, S II λ1250.578, and Fe III λ1122.524. O I λ1302.169 and Si II λ1526.707 are strong transitions revealing the weaker absorption components along each sight line, while S II λ1250.578 is a weaker transition that reveals the velocity structure of the stronger absorption components. Si II and S II trace mostly the warm neutral gas (WNM), although a fraction may arise in the warm ionised medium (WIM). O I is one of the best tracers of H I because the ionisation fraction of O is coupled to that of H via resonant charge-exchange reactions; hence, O I should trace only neutral gas along the line of sight. Fe III λ1122.524 is found mostly in the WIM, and therefore is an excellent substitute for Hα emission measurements.

In Figs. 1 to 4, we show the observed flux distribution in the vicinity of the highly ionised species with our adopted continuum fits (see the next sections for a full description of the continuum placement for those species), while in Figs. 5 and 6, we show the normalised profiles of the weakly and highly ionised species. The continuum near Si II is modeled with a straight line. The continuum near O I and S II are fitted with low-order Legendre polynomials. For the weakly ionised species, the most complicated continuum placement is near Fe III because of very strong stellar wind features from Si IV and P V. Near this transition, very high-order Legendre polynomials ($d \gtrsim 5$) must be used, and this results in a large uncertainty in the continuum placement (see Figs. 5 and 6). However, the velocity centroids of the LMC Fe III components should not be much affected by the continuum placement, at least near the core of the absorption line.

This set of lines of sight provides an opportunity to compare the highly ionised species in various environments from the Galactic halo to the LMC. Insight on the highly ionised species at lower velocity is important in its own right, but similarities (or lack thereof) in the high-ion kinematics and ratios in the MW and LMC can provide further insight on the origin(s) of the highly ionised species in the LMC. In Figs. 5 and 6, absorption for the various ions is observed from the MW to the LMC velocities. These profiles can be separated naturally in four main components: (1) the MW component (roughly $v_{\mathrm{LSR}} \lesssim 30$ $\mathrm{km\,s^{-1}}$), (2) the intermediate-velocity component (IVC with roughly $30 \lesssim v_{\mathrm{LSR}} \lesssim 100$ $\mathrm{km\,s^{-1}}$), (3) the high-velocity component (HVC with roughly $100 \lesssim v_{\mathrm{LSR}} \lesssim 175$ $\mathrm{km\,s^{-1}}$), and (4) the LMC components (roughly $v_{\mathrm{LSR}} \gtrsim 175$ $\mathrm{km\,s^{-1}}$). Here, we follow the definition of IVC and HVC from Wakker (1991). We will argue that the IVC is closely connected to the MW, but the high-velocity component may be an HVC with respect to the MW or may have an LMC origin.

2.5 Measurements of column densities, velocities, and line widths of the highly ionised species

To estimate the column densities in this work, we use the atomic parameters compiled by Morton (2003).

2.5.1 O VI *measurements*

Our O VI measurements are based on an analysis of the 1031.926 Å transition. The O VI λ1037.617 line is always contaminated by C II, C II*, and H_2 lines, and therefore cannot be used. The O VI λ1031.926 absorption in the Galactic component can be contaminated by molecular lines from the Milky Way and LMC and in principle by Cl I λ1031.507. However, Cl I is at -122 $\mathrm{km\,s^{-1}}$ and is only strong if the molecular fraction is high. We searched for the presence of Cl I λ1004.668 in our four sight lines, which has a strength similar to Cl I λ1031.507, and found none at Galactic or LMC velocities.

Three molecular lines can contaminate O VI λ1031.926. The HD 6–0 R(0) λ1031.912 is at -4 $\mathrm{km\,s^{-1}}$ relative to O VI in the restframe. No absorption from HD 3–0 R(0) through 8–0 R(0)

Table 2. Summary of AOD measurements

Ion	v_a ($\mathrm{km\,s^{-1}}$)	b_a ($\mathrm{km\,s^{-1}}$)	$\log N_a$ ($\mathrm{cm^{-2}}$)	Δv ($\mathrm{km\,s^{-1}}$)
		Sk−65°22		
O VI	258.9 ± 1.7	49.6 ± 1.6	14.14 ± 0.02	LMC [187,350]
	128.1 ± 1.0	37.8 ± 1.2	13.98 ± 0.02	HVC [88,187]
	53.0 ± 0.5	22.9 ± 0.6	13.95 ± 0.02	IVC [23,88]
	-3.0 ± 0.6	25.9 ± 0.4	13.85 ± 0.03	MW [–45,23]
N V	···	···	< 13.26	LMC [187,350]
	···	···	< 13.26	HVC [88,187]
	···	···	< 13.20	IVC [23,88]
	···	···	< 13.27	MW [–45,23]
		Sk−67°211		
O VI	251.2 ± 2.3	53.9 ± 2.6	14.20 ± 0.02	LMC [180,355]
	129.1 ± 1.6	32.5 ± 1.3	13.87 ± 0.02	HVC [100,182]
	58.2 ± 1.1	26.9 ± 0.8	14.13 ± 0.02	IVC [30,100]
	3.8 ± 1.5	22.2 ± 2.0	13.97 ± 0.03	MW [–43,30]
N V	···	···	< 13.26	LMC [180,355]
	···	···	< 13.12	HVC [100,182]
	···	···	< 13.11	IVC [30,100]
	···	···	< 13.17	MW [–43,30]
		Sk−69°246		
O VI	215.7 ± 2.1	46.3 ± 3.5	14.36 ± 0.09	LMC [139,302]
	103.1 ± 2.7	15.1 ± 4.9	13.55 ± 0.20	HVC [85,139]
	62.7 ± 2.2	17.4 ± 2.4	13.59 ± 0.10	IVC [41,85]
	5.5 ± 1.4	32.2 ± 2.1	13.96 ± 0.10	MW [–61,41]
N V	···	···	< 13.40	LMC [139,302]
	···	···	< 13.20	HVC [85,139]
	···	···	< 13.26	IVC [41,85]
	···	···	< 13.61	MW [–61,41]
		Sk−71°45		
O VI	227.3 ± 1.2	53.4 ± 1.5	14.37 ± 0.02	LMC [162,320]
	143.0 ± 0.9	32.5 ± 0.7	14.12 ± 0.02	HVC [104,183]
	67.7 ± 0.8	31.2 ± 0.6	14.20 ± 0.02	IVC [26,104]
	-0.2 ± 1.4	26.0 ± 1.5	13.77 ± 0.02	MW [–51,26]
N V	···	···	< 13.51	LMC [162,320]
	···	···	< 13.16	HVC [104,183]
	···	···	< 13.21	IVC [26,104]
	···	···	< 13.22	MW [–51,26]

Note: Refer to §§2.5.1,2.5.2 for more details on these measurements.

Table 3. C IV and Si IV fit results

Ion	v ($\mathrm{km\,s^{-1}}$)	b ($\mathrm{km\,s^{-1}}$)	$\log N$ ($\mathrm{cm^{-2}}$)	Cloud
		Sk−65°22		
C IV	271.7 ± 1.7	23.9 ± 2.7	13.59 ± 0.05	LMC
	265.4 ± 0.5	6.1 ± 1.2	13.45 ± 0.07	LMC (H II)
	105.1 ± 13.9	24.4 ± 18.2	13.11 ± 0.09	HVC
	43.1 ± 0.6	17.3 ± 0.9	13.84 ± 0.02	IVC
	-11.0 ± 1.1	13.2 ± 1.8	13.35 ± 0.04	MW
Si IV	274.1 ± 1.0	24.0 ± 1.5	13.20 ± 0.03	LMC
	269.0 ± 0.3	6.7 ± 0.5	13.25 ± 0.03	LMC (H II)
	135.6 ± 5.4	41.4 ± 10.2	12.59 ± 0.07	HVC
	47.3 ± 0.8	17.9 ± 1.2	12.96 ± 0.03	IVC
	-10.3 ± 0.4	10.7 ± 0.8	12.96 ± 0.02	MW
		Sk−67°211		
C IV	272.2 ± 0.3	11.4 ± 1.0	$(>)15.94 \pm 0.32$	LMC (H II)
	251.2 ± 3.4	43.1 ± 2.9 :	13.80 ± 0.05 :	LMC
	113.2 ± 4.9	41.0 ± 8.3	13.48 ± 0.07	HVC
	47.9 ± 6.7	22.9 ± 6.8	13.78 ± 0.22	IVC
	14.0 ± 5.9	23.7 ± 4.3	13.89 ± 0.16	MW
Si IV	276.2 ± 0.3	10.6 ± 0.9	$(>)15.09 \pm 0.25$	LMC (H II)
	262.0 ± 1.5	37.4 ± 1.5	13.53 ± 0.03	LMC
	38.7 ± 1.6	31.7 ± 2.3	13.29 ± 0.03	IVC
	0.1 ± 0.7	10.5 ± 1.2	12.90 ± 0.05	MW
		Sk−69°246		
C IV	214.1 ± 0.5	16.7 ± 1.4	$(>)14.28 \pm 0.02$	LMC (H II)
	213.5 ± 1.8	37.0 ± 7.1 :	13.90 ± 0.14 :	LMC
	98.6 ± 3.5	20.7 ± 7.9	13.09 ± 0.09	HVC
	50.2 ± 1.3	14.5 ± 2.5	13.44 ± 0.05	IVC
	6.7 ± 1.0	19.6 ± 1.7	13.75 ± 0.03	MW
Si IV	218.0 ± 0.3	12.3 ± 1.2	$(>)14.23 \pm 0.08$	LMC (H II)
	214.5 ± 0.6	37.0 ± 7.1	13.72 ± 0.04	LMC
	102.4 ± 2.0	17.6 ± 3.9	12.52 ± 0.06	HVC
	51.3 ± 1.0	16.8 ± 1.9	12.85 ± 0.03	IVC
	3.6 ± 0.5	16.5 ± 0.8	13.21 ± 0.02	MW
		Sk−71°45		
C IV	221.0 ± 0.3	15.4 ± 0.5	$(>)14.56 \pm 0.03$	LMC (H II)
	128.6 :	25.0 :	13.35 :	HVC
	61.4 ± 0.9	27.6 ± 1.5	13.98 ± 0.02	IVC
	1.0 ± 1.0	13.8 ± 1.7	13.47 ± 0.04	MW
Si IV	221.2 ± 0.4	14.8 ± 0.7	$(>)14.18 \pm 0.05$	LMC (H II)
	128.6 :	25.0 :	12.85 ± 0.08	HVC
	66.3 ± 1.2	19.8 ± 2.0	13.34 ± 0.03	IVC
	-2.6 ± 1.2	12.7 ± 2.1	13.05 ± 0.05	MW

Note: The ":" symbol highlights the uncertainty in the profile fitting to the component where colon is marked. The "(>)" symbol indicates that the line is possibly uncertain due to the effects of strong saturation. See §2.5.3 for more details on these measurements.

at 1066.271, 1054.433, 1042.847, 1021.546, and 1011.457 Å was found in the spectrum of our target stars. Therefore, HD 6–0 R(0) λ1031.912 does not contaminate the O VI transition. The H_2 lines (6-0) P(3) and R(4) lines at 1031.191 and 1032.356 Å can also contaminate the O VI absorption. These are found at -214 and $+125$ $\mathrm{km\,s^{-1}}$ relative to the O VI restframe, respectively, and can arise in both the Milky Way and LMC (see Howk et al. 2002). The imprints of these lines can be clearly seen in the spectrum of Sk−65°22, Sk−69°246, Sk−71°45, but not in the spectrum of Sk−67°211. To estimate the contribution to the O VI profiles from the 6–0 P(3) and R(4) lines of molecular hydrogen, we fitted Gaussian profiles to a number of $J = 3$ and 4 transitions of H_2 with line strengths λf similar to the contaminating 6–0 line transitions. The available H_2 transitions can be found in Table 3 of Howk et al. (2002). We have used only H_2 lines present in LiF 1A to minimise any effects of changes in the shape of the instrumental line spread function. While saturation effects may be significant, the choice of lines with similar λf circumvent in great part such problems (see Howk et al. 2002, Wakker et al. 2003).

A difficulty in assessing the interstellar O VI absorption is that the O VI stellar component predominantly associated with the wind of the star can produce a complicated continuum. Furthermore stellar wind variability can change the shape of the continuum and produce discrete absorption components (DACs) that can mimic O VI interstellar absorption (Lehner et al. 2001). The matter is complicated by the fact that we cannot use interstellar O VI λ1037.617 (see above). To evaluate the effects of the stellar wind, we considered the spectra of O VI $\lambda\lambda$1031.926, 1037.617 over a large velocity range in the O VI vicinity following Lehner et al. (2001). We note that there is no observed variation between the different exposures that were used to produce the final spectra. We review the continuum placement and possible contamination from H_2 and stellar wind features for each star:

Sk−65°22: Its stellar wind has a terminal velocity $v_\infty = -1350$ km s^{-1}, which is less in absolute value than the 1650 km s^{-1} velocity separation between the lines of the O VI doublet. The interstellar measurements are therefore not strongly affected by DACs (Lehner et al. 2001). We note that the stellar O VI profiles can be observed predominantly in both lines near -1000 km s^{-1}. We are therefore confident that the stellar continuum near O VI λ1031.926 can be simply modeled as shown in the top panel of Fig. 1. We also show in this figure the H_2 model, where the Galactic component is weaker than the LMC component.

Sk−67°211: This O2 supergiant star has the simplest stellar continuum near O VI in our sample displaying a very prominent P-Cygni profile with $v_\infty = -3600$ km s^{-1} (see Fig. 2). The effect of DACs on the local continuum is negligible since DACs are only strong and narrow near v_∞ (Lehner et al. 2001). The H_2 contamination is also insignificant towards this star.

Sk−69°246: This is certainly the most complicated star in our sample for estimating the interstellar O VI. At a terminal velocity of $v_\infty = -1847$ km s^{-1}, DACs from the O VI λ1037.617 may be present in the galactic and LMC components of O VI λ1031.926. Moreover, at such terminal velocity, the wind features from O VI λ1031.926 are lost in H I Lymanβ, making it impossible to identify features that may be present in the weaker member of the doublet using the stronger member. Therefore, it may be possible that the O VI λ1031.926 interstellar profile is contaminated. We make the assumption it is not. The continuum placement is also uncertain. In Fig. 3 (top-panel) we show two likely continua. Using the H_2 modeling, the continuum cannot be lower than the solid continuum, otherwise we would underestimate the amount of the H_2 in the LMC component.

Sk−71°45: This star has a large terminal velocity ($v_\infty = -2500$ km s^{-1}), and therefore the interstellar O VI profile is unlikely to be contaminated by a DAC. The continuum is well modeled with low-order polynomial function (see Fig. 4). The Galactic H_2 is stronger than the LMC component towards this star.

The O VI absorption does not present distinct components, as can be observed in the profiles of the other ions. We adopted the apparent optical depth (AOD) method of Savage & Sembach (1991) to estimate the column density (N_a), velocities (v_a), and line widths (b_a) of O VI. The absorption profiles were converted into apparent column densities per unit velocity $N_a(v) = 3.768 \times 10^{14} \ln[F_c/F_{\rm obs}(v)]/(f\lambda)$ cm^{-2} (km s^{-1})$^{-1}$, where F_c is the continuum flux, $F_{\rm obs}(v)$ is the observed flux as a function of velocity, f is the oscillator strength of the absorption and λ is in Å. The values of v_a, b_a, $\log N_a$ are obtained from $v_a = \int v N_a(v) dv / N_a$, $b_a = [2 \int (v - \bar{v}_a)^2 N_a(v) dv / N_a]^{1/2}$, and $N_a = \int N_a(v) dv$ (see Sembach & Savage 1992).

The O VI absorption profiles do not contain easily distinguished absorbing components, gas associated with the LMC and gas at lower velocities is usually easily separated. An important aspect of our investigation involves studying the kinematical relationships between the high and low ions and the column density ratios of the highly ionised species. We used the C IV and Si IV profiles to determine velocity integration limits for O VI that would allow us to crudely separate the different components (MW, IVC, HVC, and LMC).

The measurements for O VI are presented in Table 2. For Sk−69°246, we adopt the mean results of the high and low continua. The listed $\pm 1\sigma$ errors are from a quadrature addition of the statistical error and the continuum placement error. The 1σ errors may be slightly underestimated (by no more than 0.05 dex in the log of the column density although usually lower) because they do not include systematic from the removal of the H_2 contamination. Finally, note that saturation is unlikely to affect our measurements since the broadening of O VI is greater than the instrumental broadening of *FUSE*.

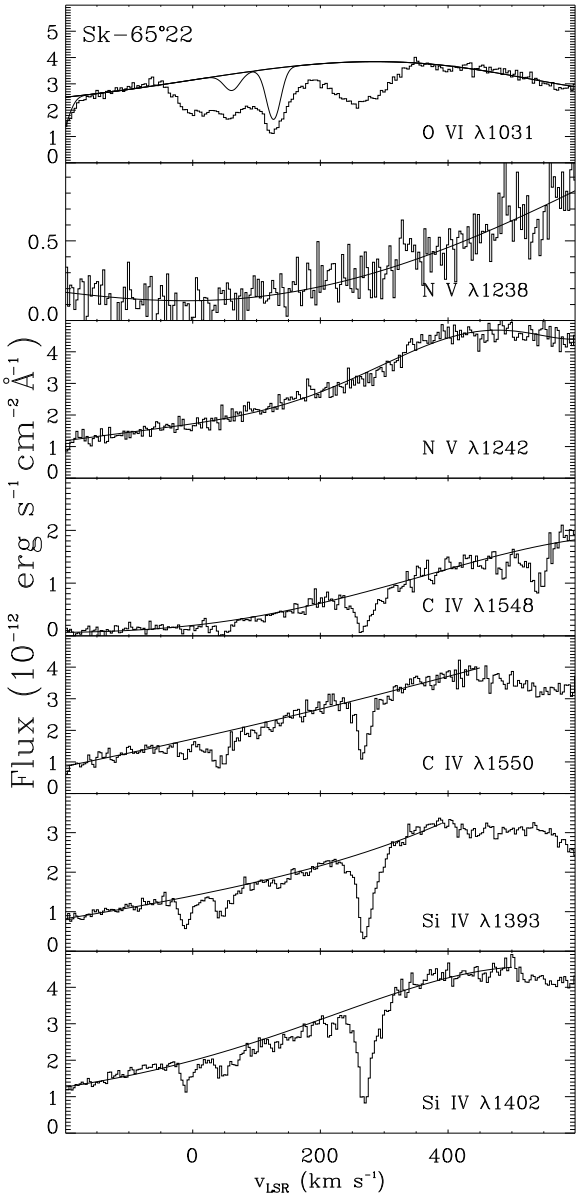

Figure 1. Plots of several highly ionised species in flux unit against the LSR velocity towards Sk−65°22. The solid line is the continuum to the interstellar line. In the O VI panel, we also the model to the H_2 line (6-0) P(3) and R(4) lines at 1031.191 and 1032.356 Å.

2.5.2 *N* V *measurements*

The interstellar N V measurements are the most straightforward because the strong stellar wind makes the continuum placement simple. Mg II λ1239.925 is at 270 km s^{-1} relative to N V λ1238.810, and therefore can contaminate the LMC component of the strong line of the doublet (see panel 2 in Fig. 2).

No interstellar Galactic or LMC N V is detected towards any of the stars in our sample. The flux is much higher in the weaker

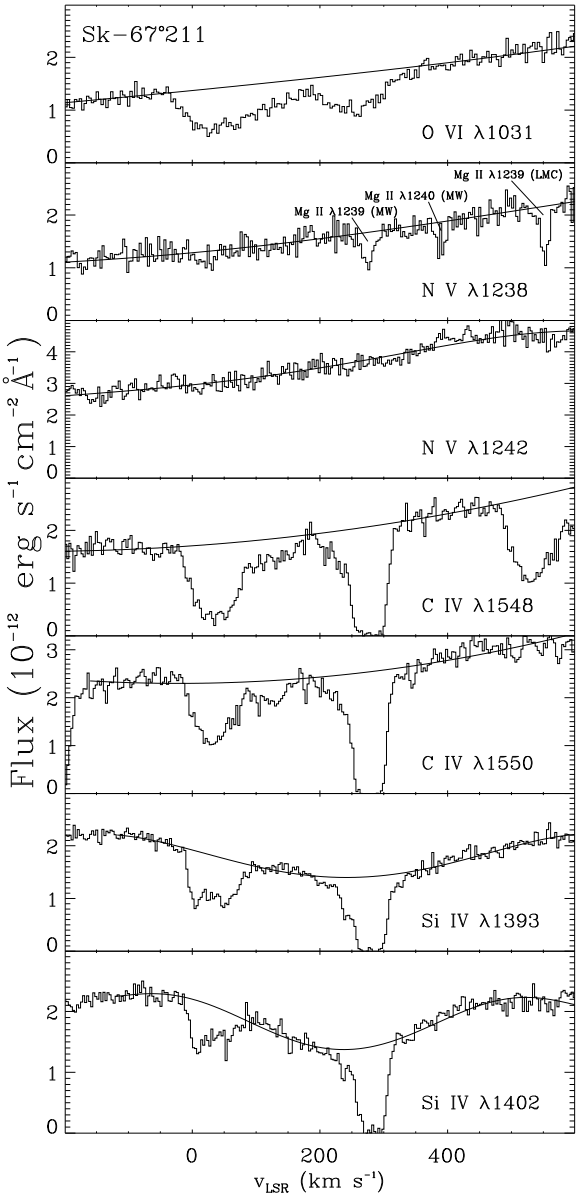

Figure 2. Same as Fig. 1 but towards Sk−67°211.

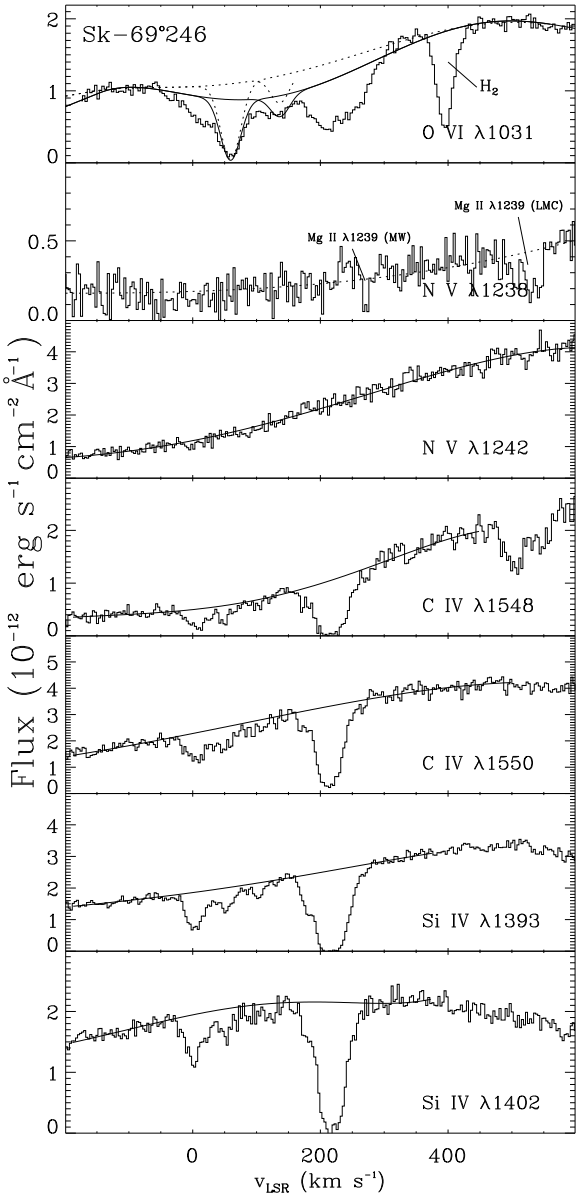

Figure 3. Same as Fig. 1 but towards Sk−69°246 (the dotted line shows another possible choice for the continuum).

transition at 1242.804 Å than in the transition at 1238.810 Å, and therefore N V λ1242.804 produces better upper limits. We report the 3σ upper limit to the column density in Table 2 by assuming the line is on the linear part of the curve of growth.

2.5.3 C IV *and Si* IV *measurements*

For C IV and Si IV, the continuum placement and the measurements of v, N, b can be constrained by considering both lines of the doublet. The absorption profiles of these ions appear also to be separated into several components rather than the single broad absorption observed in the O VI line profile. Furthermore the C IV and Si IV profiles reveal that in most cases the absorption of these ions is coupled, i.e. both ions show very similar profiles. These facts motivated us to use a Voigt profile fitting method. The fit results and the errors were obtained using the Voigt component fitting software of Fitzpatrick & Spitzer (1997). The fit results listed are based on a simultaneous fit to both members of the C IV doublet on one hand and the Si IV doublet on the other hand. However, we choose not to fit the C IV and the Si IV profiles simultaneously to avoid making an a priori assumption that these two ions trace the same gas. Rather, we prefer to show if this is the case (or not) *a posteriori*. For the STIS E140M instrumental spread function we adopted the profile from the STIS Instrument Handbook (Profitt et al. 2002). Data taken through the $0\farcs2 \times 0\farcs2$ slit have an line spread function with a narrow core and a broader halo.

While we do not present the results of the AOD measurements for C IV and Si IV, we undertook them to cross-check the validity of the profile fitting results. We find very similar results between the AOD and profile fitting methods for the MW and IVC components. For the HVC component, the column densities of C IV and Si IV could be 0.05–0.2 dex higher with the AOD measurements because the velocity interval over which the profile was integrated

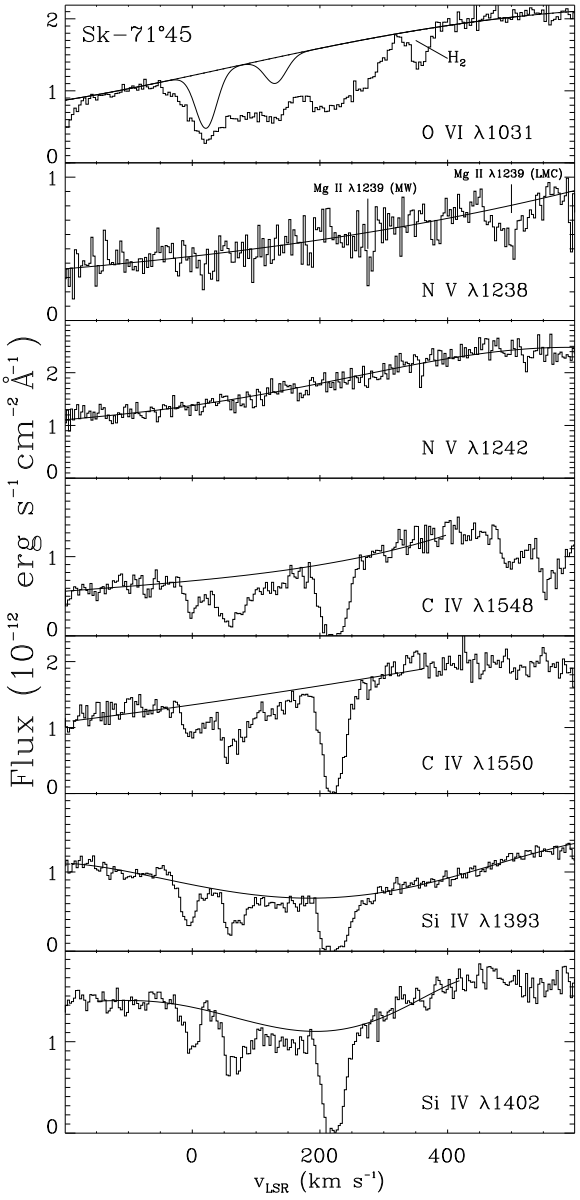

Figure 4. Same as Fig. 1 but towards Sk−71°45.

was larger than the breadth of the model. Hence, the profile fits to the HVC component are uncertain, and the AOD column density ratios (see §2.6) are more reliable since there is no assumption on the profile of the absorption line. For the strong LMC components, the AOD provided in general a lower limit in agreement with the profile fitting measurements; and in the cases where the LMC components were essentially resolved (C IV and Si IV towards Sk−65°22 and C IV towards Sk−69°246), the AOD and profile fitting gave the same results within the 1σ errors.

Below, we provide further insights on the choices of the continua and component fitting for each line of sight.

Sk−65°22: The C IV stellar wind is really strong, reducing subsequently the flux near the MW component of the C IV λ1548.195 (see Figs. 1 and 5). For Si IV, the chosen continuum is somewhat intermediate between plausible slightly higher and lower continua, but within the 1σ errors the results can be reproduced by either solution. The MW, IVC, and HVC absorption can each

Table 4. Temperatures and column density ratios

Sight line	T (10^5 K)	N(C IV)/N(Si IV)	N(O VI)/N(C IV)
LMC – H II region/Superbubble			
Sk−65°22	$\leqslant 0.27$	1.6 ± 0.3	... [a]
Sk−67°211	$(<)0.2 \pm 0.4$	$7.1 \pm {}^{9.5}_{4.8}(:)$	... [a]
Sk−69°246	$(<)1.6 \pm 0.7$	$1.1 \pm 0.2(:)$	... [a]
Sk−71°45	$(<)0.2 \pm 0.3$	$2.4 \pm 0.3(:)$	... [a]
LMC – not associated with H II region			
Sk−65°22	< 4.2	2.5 ± 0.3	3.6 ± 0.5
Sk−67°211	6.0 ± 3.0	1.9 ± 0.3 :	2.5 ± 0.3 :
Sk−69°246	< 10	1.5 ± 0.5 :	3.4 ± 1.4 :
HVC			
Sk−65°22	< 4.4	3.3 ± 1.0	7.4 ± 1.6
Sk−67°211	< 12	...	2.5 ± 0.4
Sk−69°246	1.5 :	3.7 ± 0.9	2.9 ± 1.7
Sk−71°45	...	3.2 : $\pm$0.7 :	5.9 ± 0.7
IVC			
Sk−65°22	< 2.2	7.6 ± 0.6	1.3 ± 0.1
Sk−67°211	< 3.8	...	2.3 ± 1.6
Sk−69°246	< 1.6	3.9 ± 0.6	1.4 ± 0.4
Sk−71°45	4.7 ± 1.4	4.4 ± 0.4	1.7 ± 0.1
MW			
Sk−65°22	0.8 ± 0.4	2.5 ± 0.3	3.2 ± 0.4
Sk−67°211	< 1.9	...	1.2 ± 0.5
Sk−69°246	1.5 ± 0.9	3.5 ± 0.3	1.6 ± 0.4
Sk−71°45	0.4 ± 0.9	2.6 ± 0.4	2.0 ± 0.2

Note: The temperatures are derived from the *b*-values of C IV and Si IV. The ":" symbol indicate some uncertainty in the result that is not reflected by the formal errors deduced from the measurements. The "$(<)$" symbol indicates that these lines are strong and may be composed of several components. The "$(:)$" symbol indicates that these lines are saturated and therefore the ratio is more uncertain than the formal errors from the profile fitting suggest. *a*: No O VI is found to associated with the narrow C IV component. See also §2.6 for the high ratio measurements.

be fitted well with one component. The HVC kinematical structure remains largely uncertain and unknown; there is almost certainly more than one component over the velocity range $[100, 180]$ $\mathrm{km\,s^{-1}}$. The LMC absorption is fitted well with a broad and a narrow component.

Sk−67°211: Along this line of sight, the continuum to Si IV is uncertain, especially for the HVC component. Since there is a C IV HVC component, the continua to the Si IV lines are likely to be somewhat higher than seen in Fig. 2 in the HVC range, but there is no useful constraint to indicate how much higher. Our choice of continua therefore places a firm lower limit on the Si IV column density of this HVC. A higher continuum for Si IV would also likely change slightly the IVC results. In contrast, the continuum to C IV is more straightforward. This is the only line of sight in our sample where Si IV and C IV in the MW and IVC components may trace different plasmas since the profile shapes and kinematics of Si IV and C IV are not consistent with each other. For the LMC, the C IV can be fitted well with a broad and a narrow component. For LMC Si IV absorption, the fit is not unique: one can fit the LMC absorption with a narrow and a broad component or with three narrow components. We favor the two-component fit because *a posteriori* the kinematics match well the kinematics derived for C IV. This produces further uncertainties on the physical parameters derived for Si IV, and we highlight the uncertainty in Table 3

by a colon (we discuss in §3 that a two-cloud model for the narrow C IV and Si IV components is likely).

Sk−69°246: While for O VI this line of sight has the most complicated continuum placement near the interstellar O VI, for C IV and Si IV the continuum placement is comparatively straightforward. For the MW, IVC, and HVC, we again use a single cloud model for each of these components. The C IV λ1548.195 may suggest a two-component structure at about 3 and 25 $\mathrm{km\,s^{-1}}$, and a narrower component for the IVC, but within the S/N and considering the other transition, we did not manage to improve statistically the fit with such a model. For the LMC, we used again two components. Yet a combination of two narrow or narrow and broad components can reproduce well the observed profiles. For C IV, the reduced-χ^2 are essentially the same, 1.00 and 1.03 for the narrow-narrow fit and narrow-broad fit, respectively. For Si IV, the reduced-χ^2 is slightly better for the narrow-broad component fit compared to the narrow-narrow component fit, 1.12 compared to 1.27, respectively. The centroid of the broad component of Si IV and C IV matches well the centroid of the broad O VI absorption. The broadenings of O VI and C IV also appear compatible within 1σ. Finally, the extra absorption observed in the red wing of C IV and Si IV can only be reproduced adequately with a broad component, putting more weight on this solution. We therefore favor the broad-narrow component fit, but we highlight the uncertainty in the broad component in Table 3 by a colon. We note that the LMC absorption lines are very strong; if a narrower component is present in the profile, the column densities could be uncertain by an order of magnitude.

Sk−71°45: This is the second giant star having a similar stellar spectrum near Si IV to that of Sk−67°211. Although we had less difficulty finding continua that appear satisfactory for both lines of the Si IV doublet than for Sk−67°211, the true shape of the continua remains unknown and the quoted errors do not adequately reflect this systematic uncertainty. As for the other lines of sight, the continua for the C IV doublet lines are comparatively straightforward to model. The C IV and Si IV absorption profiles are modeled with a single component for each cloud. For the HVC, we fixed the *b*-value for both ions; the centroid velocity for Si IV was also fixed to the C IV velocity. If b is not fixed, the fitting procedure tends to fit an unrealistically broad component. The LMC component of Si IV λ1393.755 appears to have a wing not reproduced by the fit. However, this is not observed in the other transition, and we attribute this to the continuum placement. The addition of another LMC component to model this absorption fails to produce an adequate fit to the lines. The LMC lines are very strong and if a narrower component is present in the profile (and it is likely the case, see discussion in §3), the column densities could be again uncertain by an order of magnitude.

2.6 Column density ratios of the highly ionised species

Theoretical models predict the highly ionised species are produced via a range of mechanisms, such as in shocks or in interfaces between different temperature gas, with conductive heating, turbulent mixing, or in radiative cooling gas (see references in Table 5 and summaries from Spitzer 1996, Fox et al. 2003 Indebetouw & Shull 2004). O VI is of prime importance since in the galactic environments, it is produced mainly via collisional processes. In contrast Si IV and C IV can be produced by photoionisation. If there is a kinematical relationship between the highly ionised species, the ratio of the high-ion column densities can be used to determine which physical mechanism is predominant in the ISM, if any, and how the mechanisms responsible for producing the highly ionised species may change in different galactic environments.

Two methods were used to determine the ratios of highly ionised species. In Table 4, the ratios of the column densities of C IV and Si IV obtained from the profile fitting are summarised. We also measured systematically the O VI column densities and N V column density limits by using the velocity extent of each cloud defined by the profile fitting of C IV and Si IV. The ratios $N(\mathrm{O\ VI})/N(\mathrm{C\ IV})$ derived from these measurements are listed in the last column of Table 4. Since the O VI absorption profiles do not break up into easily-identifiable clouds or blends of clouds like C IV and Si IV, O VI may or may not be associated with the other ions.

In the second method, we compare the apparent column density profiles over a certain velocity range that is listed in Table 5. This method does not make any physical assumption of the properties of the gas. We separate the profiles in several velocity ranges corresponding to various clouds obtained in the profile fitting (MW, IVC, HVC, LMC). We give in Table 5 the range of ratios that spans the full range of the $\pm1\sigma$ errors. If only an upper limit is available, the 3σ upper limit and the apparent column density were estimated over the same velocity range.

There is a good agreement between both methods for the MW and IVC components. This is not surprising since the MW and IVC components are strong, but not saturated, and well separated from one another and from other component blends. The component fits to the C IV and Si IV HVC profiles are not always unique due to the broad wing-like shape of the HVC absorption. Yet, there is a rough agreement between the AOD and profile fitting methods. Because the HVC profiles are not Gaussian, we favor the AOD results over this velocity range. Hereafter, we discuss separately the quite narrow components of the highly ionised species in the LMC and the broad LMC components, which we assume includes all of the O VI given the lack of narrow absorption in this ion.

For the LMC broad component, the ratios derived from the AOD and profile fitting methods can generally not be compared: the AOD estimates the ratios in the wing of the absorption where it is not contaminated by the narrow components observed in C IV and Si IV, while the profile fitting models the broad absorption even in regions where the strong narrow absorption is present (see Figs. 5 and 6). In two cases, the comparison between the two methods can be made because the AOD estimates are made over a large fraction of the profile: Sk−67°211 ($v_{\rm LSR} = [180, 230]$ $\mathrm{km\,s^{-1}}$) and Sk−69°246 ($v_{\rm LSR} = [139, 190]$ $\mathrm{km\,s^{-1}}$). The AOD O VI/C IV ratios are in excellent agreement with those derived with the profile fitting for these sight lines. For the LMC narrow component, the only line of sight for which the ratios appear secure is Sk−65°22; along this sight line the narrow component of C IV and Si IV is not too strong and, therefore, the profiles can be modeled without too much uncertainty. For the other lines of sight, the high-ion ratios of the narrow component are uncertain because C IV and Si IV are saturated. We discuss the high-ion ratios and implications in §4.

3 OVERVIEW OF THE HIGH-ION KINEMATIC PROPERTIES

3.1 Kinematics of the LMC absorption profiles

Interstellar absorption from the low- and high-ionisation species is always detected over the full range of velocities from the Milky Way to the LMC (except for N V) along the four lines of sight in

Table 5. Ratio of the highly ionised species from AOD comparison

Model/Sight line	N(O VI)/N(Si IV)	N(O VI)/N(C IV)	N(O VI)/N(N V)
	Models		
Collisional Ionisation Eq. (CIE)	$\geqslant 111$	3.7–200	0.65–55.6
Radiative Cooling (RC)	$\geqslant 76.9$	5.9–27.8	11.1–18.9
Conductive Interface (CI)	$\geqslant 17.2$	1.1–23.8	2.0–15.4
Turbulent Mixing Layers (TMLs)	0.8–11.5	0.06–1.0	1.7–5.9
Shock Ionisation (SI)	$\geqslant 5.6$	0.96–62.5	19.6–32.3
Supernova Remnant (SNR)	$\geqslant 74.4$	5.2–8.4	11.9–16.0
Stellar Wind (SW)	100	6.3	15.8
Halo SNR	···	0.42–5.0	3.0–11.1
	LMC – H II region		
Sk−65°22	$\lesssim 1.0$	$\lesssim 0.8$	···
Sk−67°211	< 0.3	< 0.1	···
Sk−69°246	< 0.8	< 0.4	···
Sk−71°45	< 0.5	$\lesssim 0.2$	···
	LMC – not associated with H II region		
Sk−65°22 [187,232]	> 37	> 5.4	> 3
Sk−67°211 [180,230]	···	2.2–5.1	> 7
Sk−69°246 [139,190]	4.6–10.7	1.7–5.0	> 10
Sk−71°45 [162,190]	···	5.4–9.1	> 9
Sk−71°45 [260,320]	···	> 11.0	> 6
	HVC		
Sk−65°22 [88,187]	20.4–57.5	4.7–9.5	> 5
Sk−67°211 [100,182]	···	2.9–4.3	> 6
Sk−69°246 [85,139]	8.1–30.1	1.4–5.6	> 2
Sk−71°45 [104,183]	···	4.9–7.2	> 9
	IVC		
Sk−65°22 [23,88]	4.0–12.6	0.4–1.3	> 6
Sk−67°211 [30,100]	7.9–20.1	0.9–2.2	> 11
Sk−69°246 [41,85]	3.9–7.9	0.9–1.7	> 2
Sk−71°45 [26,104]	3.2–20.0	1.0–3.2	> 10
	MW		
Sk−65°22 [–45,23]	2.5–11.2	1.1–3.2	> 4
Sk−67°211 [–43,30]	4.0–7.1	1.0–1.8	> 6
Sk−69°246 [–61,41]	3.2–6.3	1.1–2.0	> 2
Sk−71°45 [–51,26]	2.5–7.1	1.0–1.8	> 4

Note: See §2.6 for the high ratio measurements. References for the models: CIE – Sutherland & Dopita (1993) for gas temperature $T = (2\text{–}5) \times 10^5$ K; RC – Edgar & Chevalier (1986); CI: Borkowski, Balbus, & Fristrom (1990) for magnetic field orientations $\theta = 0\text{–}85°$ and interface gas ages 10^{5-7} yr; TML – Slavin, Shull, & Begelman (1993) for a gas flow in the range 25–100 $\mathrm{km\,s^{-1}}$ and temperature of postmixed gas in the range $\log T = 5\text{–}5.5$; SI – Dopita & Sutherland (1996) for $150 < v_{\rm shock} < 500$ $\mathrm{km\,s^{-1}}$ and a magnetic parameter less 4 $\mu\mathrm{G\,cm^{-3/2}}$; SNR – Slavin & Cox (1992) for SNR ages $10^{5.6-6.7}$ yr; SW – Weaver et al. (1977); Halo SNR –Shelton (1998) for SNR ages $10^{6.0-7.2}$ yr.

Table 6. Summary of the velocity centroids in the LMC

Name	v(Hα) ($\mathrm{km\,s^{-1}}$)	v(Fe III) ($\mathrm{km\,s^{-1}}$)	v(O VI) ($\mathrm{km\,s^{-1}}$)	v(C IV) (narrow) ($\mathrm{km\,s^{-1}}$)	v(C IV) (broad) ($\mathrm{km\,s^{-1}}$)	Environments[a]
Sk−65°22	270 ± 15	270.6 ± 1.3	258.9 ± 1.7	265.4 ± 0.5	271.7 ± 1.7	Faint H II region
Sk−67°211	285 ± 17	286.3 ± 1.0	251.2 ± 2.3	272.2 ± 0.3	251.2 ± 3.4	H II region
Sk−69°246	252	214.7 ± 3.1^a	215.7 ± 2.1	214.1 ± 0.5	213.5 ± 1.8	Superbubble (X)
Sk−71°45	227 ± 19	214.8 ± 1.8	227.3 ± 1.2	221.0 ± 0.3	···	Superbubble

Note: a: For this sight line, Fe III was fitted with a two-Gaussian component that yields for the second component $v_{\rm LSR} = 242.3 \pm 4.4$ $\mathrm{km\,s^{-1}}$.

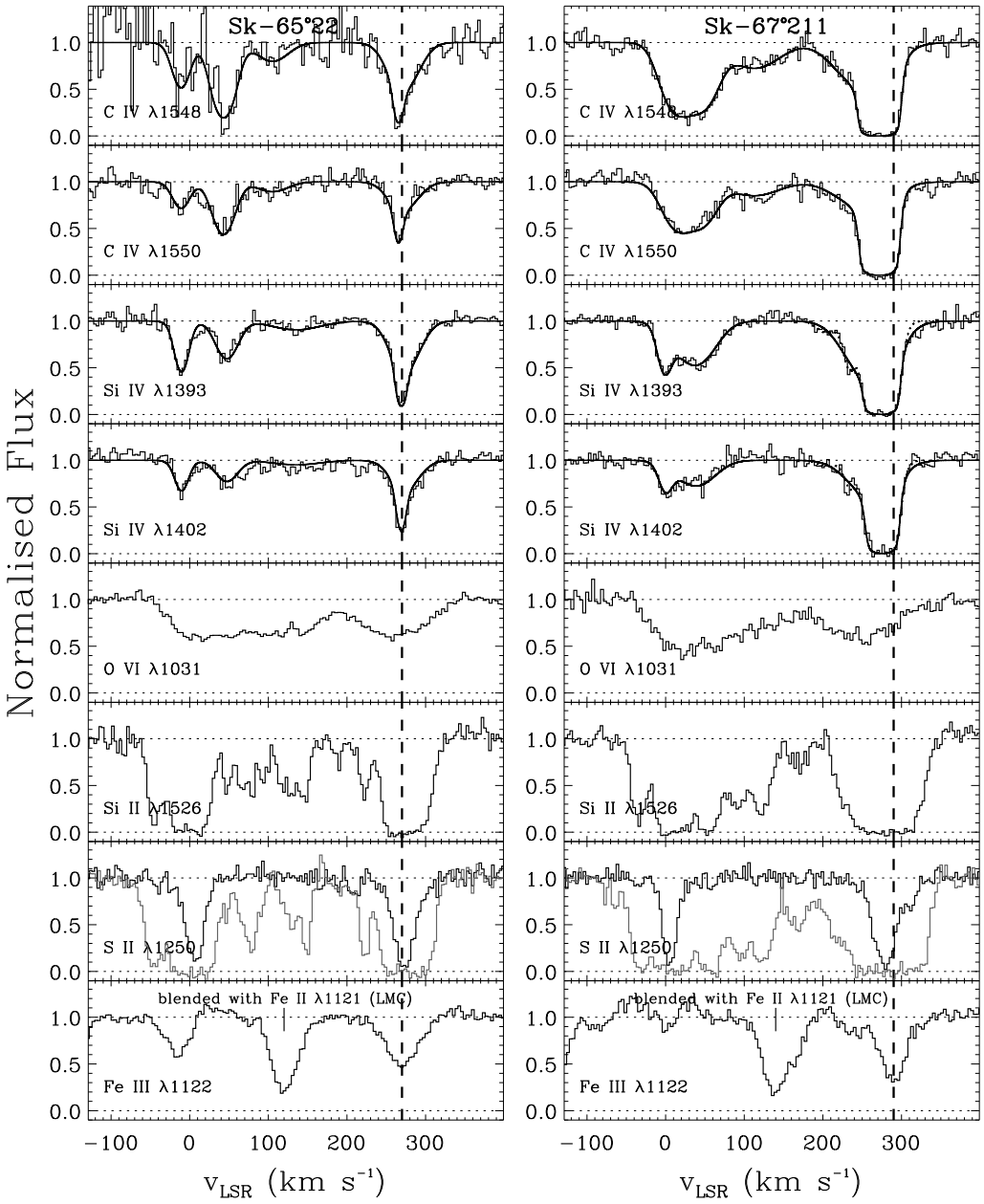

Figure 5. Normalised profiles of the selected ions observed along each line of sight. In the S II panel, the gray histogram represents the O I λ1302 absorption profile. The solid black curve shows the profile fit to the C IV and Si IV lines. We note that the continuum placement near Fe III is typically uncertain, and these profiles are shown to demonstrate only the velocity distribution of the Fe III absorption. The vertical dashed line represents the systemic Hα velocity.

our sample. In Figs. 5 and 6, we show the normalised profiles of the various species. In these figures, the vertical dashed line represents the profile-weighted average velocities measured for the Hα profiles (results from Danforth 2006 and Chu et al. 1994, see Table 6). Both superbubbles show evidence for expanding shells in Hα; the projected radial velocities of the approaching side are shown by the dotted lines in Fig. 6 (Y.-H. Chu 2006, priv. comm.; see also Chu & Kennicutt 1994). There is no obvious structure of expanding shell seen in Hα toward the other sight lines. The average velocities obtained from the Hα emission profiles agree remarkably well with the centroids measured in the Fe III profiles (see Table 6). The Fe III profiles in the spectra of Sk$-$69°246 and Sk$-$71°45 show indication of two components with one matching the systemic velocity of the Hα profile and the other matching the velocity of the expansion of the shell. The agreement between the Hα and Fe III profiles is quite remarkable given that Hα emission data probe gas in front of and behind the star while absorption spectra only probe gas in front the star.

Figs. 5 and 6 show continuous absorption at LMC velocities ($\sim$130–310 $\mathrm{km\,s^{-1}}$ towards Sk$-$65°22; $\sim$210–370 $\mathrm{km\,s^{-1}}$ towards Sk$-$67°211; $\sim$130–310 $\mathrm{km\,s^{-1}}$ towards Sk$-$69°246; $\sim$150–340 $\mathrm{km\,s^{-1}}$ towards Sk$-$71°45) for O VI, Si II, and O I. (We note that velocities $80\ \mathrm{km\,s^{-1}} \lesssim v_{\rm LSR} \lesssim 130\ \mathrm{km\,s^{-1}}$ may have an LMC origin as well; see §4.2.) Over these velocities, the O VI profiles are broad and have vaguely Gaussian shapes. The weakly ionised species consist of several narrow components.

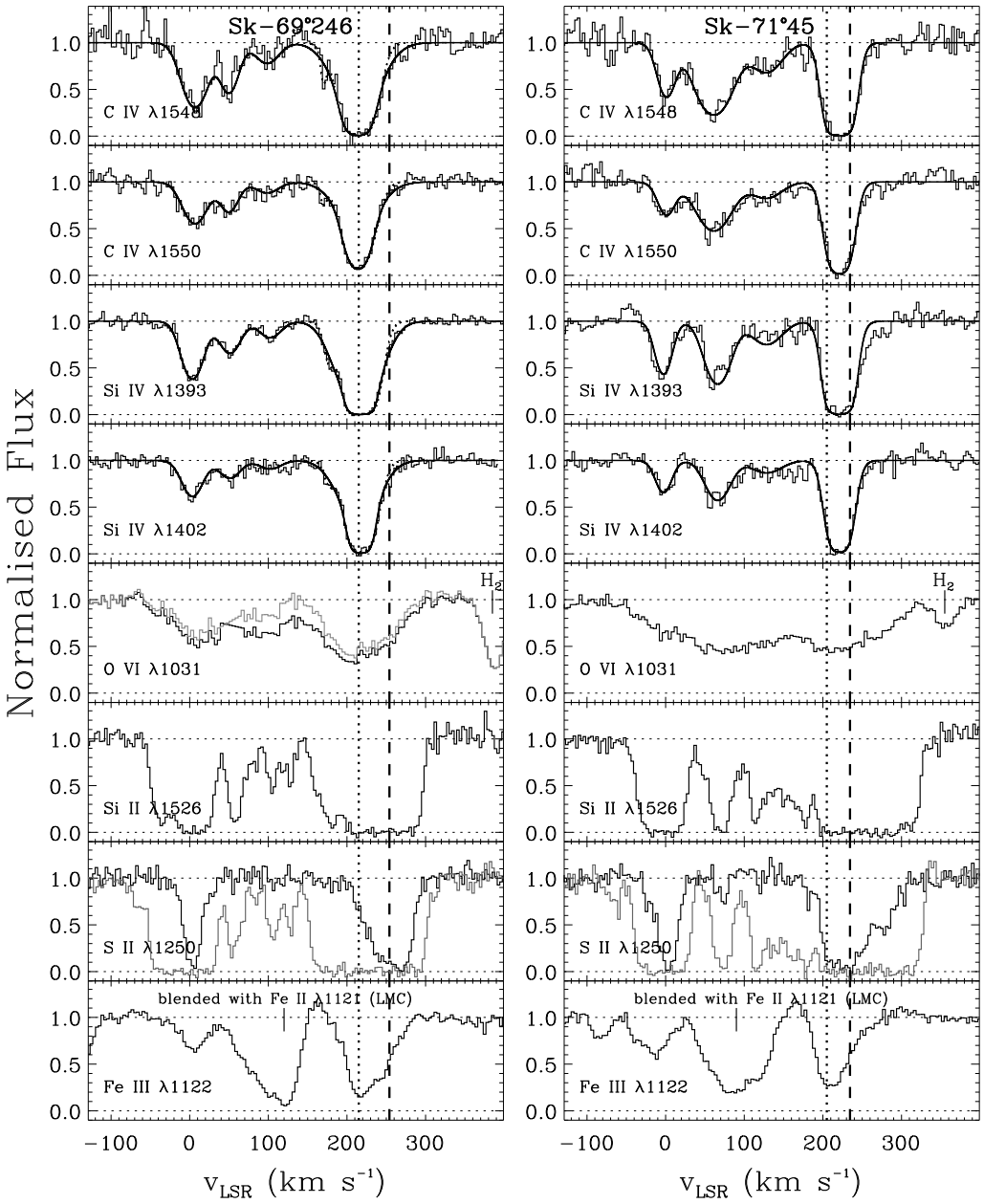

Figure 6. Same as Fig. 5 for the two sight lines Sk−69°246 and Sk−71°45. Towards Sk−69°246, we show the normalised profiles of O VI from both the high and low continua). The S II panels also include the O I λ1302 profiles. The vertical dotted line represents the expanding Hα shell velocity (Y.-H. Chu 2006, priv. comm.).

Since O VI traces much hotter gas than Si II or O I, the difference in the appearance of the profiles is expected. In contrast with the weakly ionised species, the overall kinematic morphology of the O VI profiles is quite similar between the various sight lines.

Si II and O I also reveal the presence of an IVC with respect to the LMC at $v_{\rm LSR} \sim$ 150–220 km s^{-1}, clearly separated from the main absorption by roughly -50 km s^{-1}. This LMC-IVC component possibly traces some ejecta from the LMC disk (see §4.2). The O VI absorption is always present in this IVC component. We note here that the important difference between the choice of strong transitions compared to the weaker Fe II absorption profiles used by Howk et al. (2002): the strong transitions reveal cooler, neutral and partially ionised gas traced by weakly ionised species and hot gas traced by O VI are systematically found at similar velocities.

The morphology of the C IV and Si IV profiles differs from the morphology of the O VI profiles. Along our four sight lines, a strong narrow component is observed in C IV and Si IV but not revealed in O VI. Along three sight lines, the profiles of C IV and Si IV have the strong narrow component blended with a broad component (see §2.5.3). The broad component is likely associated with some of the observed O VI. There is a good agreement between the centroids of broad C IV and Si IV components with the centroid

of the broad O VI absorption towards Sk−67°211 and Sk−69°246 (see summary in Table 6). Towards Sk−65°22 the broad component of C IV and Si IV is shifted by 12 $\mathrm{km\,s^{-1}}$ because the lower velocities observed in the O VI profile are not seen in the C IV and Si IV profiles.

In the faint H II region where Sk−65°22 is located, the centroids of the narrow components of C IV and Si IV align with those of Fe III and Hα as well as with the main component of the weaker ions (see Fig. 5). This sight line has the simplest LMC kinematics of our four. For Sk−67°211, the narrow components of the C IV and Si IV absorption profiles appear shifted to lower velocities relative to the velocities of Fe III and Hα. However, C IV and Si IV are saturated and the narrow profiles may contain more than one component. Towards Sk−69°246, the main absorption of C IV and Si IV is observed at the expanding velocity seen in Hα and Fe III. There is very little absorption in the C IV and Si IV profiles at 252 $\mathrm{km\,s^{-1}}$, which corresponds to the systemic velocity of Hα. Finally, towards Sk−71°45, also located in a superbubble, the C IV and Si IV profiles do not align with either component of Fe III, their velocities being somewhat intermediate between the systemic and expanding shell velocities observed in Fe III and Hα. The gas traced by the narrow components of C IV and Si IV, and Fe III are kinematically related in a different manner toward each sight line: there is an excellent agreement in their velocity profiles in the quiet H II region; in the bright H II region, C IV and Si IV is blue-shifted with respect to Fe III, possibly revealing an highly-ionised expanding shell; in the X-ray bright superbubble, C IV and Si IV appear to probe mostly the expanding shell seen in the Hα profile; and in the superbubble DEM 221, C IV and Si IV do not appear to directly be kinematically related to Hα, with the velocities of the highly ionised species intermediate between the expanding or systemic velocities of Hα. We finally note that weaker ions (Si II and O I for example) and higher ions (O VI) can produce absorption at these velocities.

In summary, the absorption profiles of the weakly ionised species and O VI always span the same velocity range, though the former are always found in discrete, narrow components, while the latter is broad and widespread. There is either a positive, negative, or no shift between the average velocities of O VI and weakly ionised species. However, the comparison of the average velocities of O VI with the weakly ionised species is complicated since O VI is almost certainly a blend of several components (see §3.2). The velocity extent of the C IV and Si IV LMC profiles is sometimes smaller than the O VI profile extent. The narrow LMC components of C IV and Si IV may be kinematically connected to the gas traced by Hα and the weakly ionised species (e.g., Fe III, Si II), but not in a systematic way, implying that even though the narrow components of C IV and Si IV probe cool gas ($T \lesssim 2\times10^4$ K, see below) as Fe III, their origin/production may differ, at least in some cases.

3.2 Broadening of the high-ion absorption profiles

The gas temperatures derived from the b-values of C IV and Si IV are given in Table 3. These remain quite uncertain for the LMC narrow component as the profiles are very strong, and the errors do not reflect the possibility that the profiles have more than one component. To derive these temperatures, we assume that C IV and Si IV reside in the same gas, which is supported by the compatibility in the centroids of C IV and Si IV for most clouds. In Table 3, we list the temperature of the gas derived from the observed broadening of the absorption lines. If b(C IV) $>$ b(Si IV) then T can be determined from $b = \sqrt{2kT/(Am_{\rm H}) + b_{\rm nt}^2}$, where $b_{\rm nt}$ is the non-thermal component and the other symbols have their usual meaning. If b(C IV) $<$ b(Si IV) an upper limit on the temperature can only be derived because we cannot estimate the non-thermal broadening.

For the strong, narrow LMC component (denoted LMC (H II) in Table 3), we find a good agreement between the centroids of Si IV and C IV. The Doppler broadenings suggest a temperature of 2×10^4 K along three lines of sight (towards Sk−69°246, within 2σ error, the temperature is compatible with 2–9 $\times\,10^4$ K). Since the profiles are strong and saturated towards at least Sk−67°211 and Sk−69°246, the derived b is uncertain but places a firm upper limit on the temperatures; these clouds likely have $T \lesssim 2\times10^4$ K. The non-thermal broadenings of C IV and Si IV appear to be as large as the thermal broadening if the profiles consist of a single component.

There must be little or no O VI associated with the narrow and strong C IV and Si IV components since there is no indication of a narrow component in the overall broad and smooth profile of O VI (see the limits of O VI to C IV or Si IV ratios in Table 5). Hence there is no evidence for O VI arising directly within the superbubble shells or the H II regions. We also note that these H II regions and superbubbles do not produce any detectable N V. This is not surprising since the temperatures deduced from the C IV and Si IV line-width are only a few $\times10^4$ K or less, too cool to produce any significant amount of O VI or N V.[1]

For the broad C IV and Si IV components of the LMC, their b-values imply temperatures of a few $\times10^5$ K or less. Their broadening is consistent with that of O VI, and these components likely probe hot gas. For O VI only upper limits to the temperatures can be derived, and these are always consistent with temperatures of a few 10^5 K. The broad LMC components of the highly ionised species have $b(\mathrm{LMC}) \geqslant \sqrt{b^2(\mathrm{MW}) + b^2(\mathrm{IVC})}$, suggesting that they likely trace more than two different clouds.

4 THE HIGHLY IONISED PLASMA IN THE LMC

We found that the absorption of the highly ionised species at velocities similar to the LMC disk is dominated by a narrow absorption observed in C IV and Si IV but not in the O VI. The O VI along all four sight lines is broadly distributed, and the profile fitting of C IV and Si IV reveals broad absorption in these ions along 3 of 4 sight lines. These two types of absorption components are certainly produced by different mechanisms. We discuss them separately.

4.1 The narrow absorption components

The photon flux from hot stars drops sharply above 54 eV because of the He II ionisation edge, so photoionisation by hot stars can produce Si IV (33.5 eV) and C IV (47.9 eV) but not significant N V (77.5 eV) or O VI (113.9 eV). This energetic argument was, for example, advanced by Fox et al. (2003) to explain the narrow C IV and Si IV absorption components observed towards a Galactic sight line. We show in the previous section that the broadenings

[1] N could be underabundant in the LMC H II regions (Garnet 1999, Welty et al. 1999). However, the ratios of C IV/N V for the narrow component are greater than 1.7, 478, 7.6, 10.0 towards Sk−65°22, Sk−67°211, Sk−69°249, and Sk−71°45, respectively. So even if N may be intrinsically underabundant by a factor up to 6, with such high ratio limits (especially towards Sk−67°211), the bright H II region and superbubbles do not produce any observable amount of N V.

of the C IV and Si IV imply temperatures of a few 10^4 K and likely less in the stronger features because of unresolved components. The velocities of the narrow C IV and Si IV components are consistent in two cases with the velocities of the H II region or the expanding shell as traced by Hα emission and Fe III absorption. These observed properties are in agreement with photoionisation playing an important role in the production of these ions along with Fe III and Hα. But in the two other cases, the bulk of the absorption in C IV and Si IV do not correspond to either the systemic or expanding velocities of the regions probed, suggesting that additional or different production mechanisms are in play.

The C IV/Si IV ratios in the narrow components appear always greater than 1 (from AOD and profile fitting comparisons), although we remind the reader that the Si IV continua in the spectra of Sk-67°211 and Sk-71°45 are uncertain (see §2.5.3). For Sk-67°211, Sk-69°246, and Sk-71°45, the hidden complexity within the strongly-saturated C IV and Si IV profiles are likely to have more than one component, and our column densities are thus uncertain. While the O VI/C IV and O VI/Si IV ratios are uncertain, they appear to always be smaller than unity, implying very little O VI is produced by the same mechanisms that produce the strong, narrow components of C IV and Si IV. This is further strengthened by the high C IV/N V ratios (see footnote 1).

Photoionisation models of diffuse H II regions generally produce ratios C IV/Si IV less than unity, although the addition of X-rays can boost this ratio (Black et al. 1980; Cowie, Taylor, & York 1981; Knauth et al. 2003). The b-values of the narrow C IV and Si IV components seen in our data strongly suggest, however, that photoionisation may play a role in producing this material. We have undertaken simple photoionisation models using the Cloudy code (v06.02.09; last described by Ferland et al. 1998) to test the assumption that the underlying structures may give rise to the narrow components. We calculated a model spherical H II region about a single star having properties similar to the star Sk-65°22: $\log L/L_\odot = 6.2$, $T_{\rm eff} \approx 40000$ K (from Massa et al. 2003). We adopted LMC metal abundances from Russell & Dopita (1992). Our models include a treatment of interstellar grains for heating/cooling and opacity purposes; this dust affects the abundances due to elemental depletion (see Cloudy documentation). We assumed a clearing within the inner-most parsec of the H II region and constant density outward of this radius. In general we find that such models, with an extremely bright, high temperature star, can reproduce (or exceed) the measured C IV/Si IV ratios observed in the narrow components along the sight lines in this work. We examined models without the depletion (i.e., a non-self consistent model with grains for thermal and opacity effects, but leaving all the metals in the gas phase), which verified the depletion effects did not dominate the C IV/Si IV results. These single star H II region models, while able to match or exceed our observed C IV/Si IV measurements, do not simultaneously match this ratio and the total column densities of the highly ionised species seen towards Sk-65°22. In fact, the models that produce a sufficiently high column density tend to over-predict the C IV/Si IV ratio. However, these are extremely simple models that do not take into account the other stars in the vicinity of our target objects, the complex geometries and density structures within the regions, etc. Given the high temperatures and the quite high luminosities of our target stars, as well as their locations within star forming regions in the LMC, it seems likely that direct photoionisation from OB-type star photospheres could explain the narrow C IV and Si IV along some sight lines.

Given the kinematic complexity of the other sight lines (see §3), several processes may be at work or that the structures giving rise to the absorption have complex internal kinematics. In particular, early-type stars with strong stellar wind create large cavity in the ambient ISM (Castor, McCray, & Weaver 1975). Bubbles have complex kinematics and have a mixture of hot ($T > 10^6$ K) and cool ($T < 10^4$ K) (Weaver et al. 1977). The hot gas is principally found in the shocked wind. The cooler gas mainly is found in the shell behind the conducting front following a rapid radiative cooling (see also, Shapiro & Moore 1976; Sutherland & Dopita 1993). Such process also creates an interface between the hot and cool gas at $T \sim 10^5$–10^6 K where some of the observed O VI is produced (see below). The ionisation of the outer shell depends mostly on the radiation of the central star (Weaver et al. 1977). It is interesting to note that the two hotter stars in our sample show the strongest C IV and Si IV absorption associated with an expanding shell (see §3). The stellar wind model therefore provides a qualitative explanation for part of observed narrow component associated with the outer/expanding shell. This is also supported by the recent *Chandra* observations of 30 Do, which shows that Sk-69°246 may be a colliding-wind binary with bright X-ray emission from 2.1 keV plasma (Townsley et al. 2006). However, 30 Dor and other regions of the LMC are also well known for their superbubbles created not only by stellar winds but also SNRs. The SNR models of Slavin & Cox (1992) can also produce cool highly ionised at 10^4 K. This is not surprising since the SNR and stellar wind models explore very similar physics; in the former the source of the shocked is the supernova, in the latter case, it is the central star. The stellar wind and SNR models place the expanding shell within a radius of about 30 to 100 pc from the central region. Yet, other physical scenarios might produce such cool highly-ionised gas, as well. For example, emission of a hot, cooling plasma could photoionise the gas; O VI and N V are negligible with respect to C IV and the temperature of the gas is low ($T < 10^4$ K) so the C IV and Si IV broadenings are small (Knauth et al. 2003).

In summary, in view of the kinematical differences between the various sightlines, the origins of the narrow components observed in the C IV and Si IV profiles are most likely multiple. In the spectra of Sk-67°211 and Sk-71°75, it is likely that the narrow components of C IV and Si IV are in fact at least two narrow components (hence tracing gas at $T \lesssim 10^4$ K) at the systemic and expanding shell velocities. In the spectrum of Sk-65°22, the absorption is comparatively weak and consistent with a single narrow component associated with the H II region around the star. And in the spectrum of Sk-69°246, there is only evidence of a strong absorption at the velocity of the expanding shell, showing the peculiarity of this line of sight. While the exact origins of the highly ionized species probed by the narrow components remain unknown, their properties can be chiefly associated with the stellar environments.

4.2 The broad absorption components

Towards each line of sight, the O VI LMC component is very broad with $b \sim 50\,{\rm km\,s^{-1}}$, much larger than the broadening of the Galactic plus the IVC or the temperature at which O VI peaks in abundance in CIE, implying that the LMC O VI component is composed of several kinematic components. There is evidence for broad C IV and Si IV LMC absorption components associated with the O VI towards at least 3 lines of sight. Although the velocity structure of the broad absorption is not fully known, the high-ion profiles suggest that this gas traces hot collisionally ionised gas at temperatures of a few times 10^5 K. We also showed in §3 that O VI and Si II have absorption over nearly the entire range of velocities from

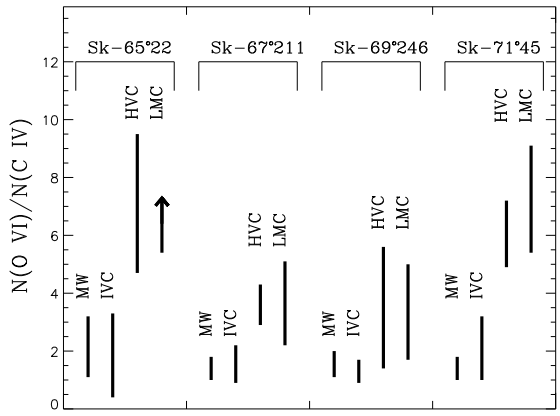

Figure 7. Summary of the column density ratios of O VI to C IV for the MW, IVC, HVC and broad LMC components towards the four sight lines, obtained from the AOD measurements (see Table 5).

-50 to $+330$ km s^{-1}. C IV and Si IV cover a smaller velocity range. In particular they do not show absorption at the lowest or highest velocities associated with the LMC. Thus, gas at the lowest and highest velocities makes a proportionately smaller contribution to the total columns of C IV and Si IV than it does in O VI.

4.2.1 Ratios of the highly ionised species

Fig. 7 shows the O VI/C IV ratio (from Table 5) along our four sight lines, separated into the four principal components: the MW ($v_{\rm LSR} \lesssim +30$ km s^{-1}), IVC ($30 \lesssim v_{\rm LSR} \lesssim 100$ km s^{-1}), HVC ($100 \lesssim v_{\rm LSR} \lesssim 175$ km s^{-1}), and broad LMC ($v_{\rm LSR} \gtrsim 175$ km s^{-1}) velocity components. Over the velocities where the narrow components discussed above are present the ratios are inferred mostly from the profile fitting (Table 4), except towards Sk-67°211 and Sk-69°246 where the absorption is weak enough that the ratios of the apparent column densities can be estimated over a portion of the absorption profiles. In the broader wings of the absorption profiles, the ratios are inferred from our AOD analysis (Table 5). For Sk-65°22, the fits to the broad components of C IV and Si IV absorption appear secure, but the fits to the broad absorption along the other sight lines are not unique (see §2.5.3). We found a good agreement between the ratios estimated from the AOD and profile fitting for Sk-67°211 and Sk-69°246, strengthening the results from the profile fitting.

While there is some room for variations in the O VI/C IV ratio as a function of velocity along a given sight line (our approach to deriving the values plotted in Fig. 7 is relatively conservative), the HVC and broad LMC components have quite similar O VI/C IV ratios, and the MW and IVC components are generally in agreement with one another, but smaller than the HVC–LMC values. The observed O VI/Si IV ratios for the LMC and HVC are roughly consistent with those found in the MW or IVC components, but the O VI/C IV ratios are generally quite a bit larger in the HVC and LMC material than in the MW or IVC material. Moreover, the O VI/C IV ratios in HVC and LMC gas seem to vary between sight lines, but the ratios in the HVC and LMC components *along a given sight line* are always very similar.

4.2.2 Evidence for outflows

The similarity of the O VI/C IV ratios between the HVC and LMC gas suggests that (i) the HVC component has its origins in the LMC, and (ii) the processes producing the highly-ionised gas in the LMC affect a large range of velocities along a given sight line in a similar manner. The first of these conclusions supports a conclusion drawn by Staveley-Smith et al. (2003) in their study of the H I structure of the LMC. These authors found that the relatively high column density clouds at velocities $v_{\rm LSR} \sim 100$–160 km s^{-1} towards the LMC are often seen projected onto H I voids in the LMC disk, and they are connected to the disk with spatial and kinematic bridges in position-velocity plots. They also note the presence of material at velocities outside the range of velocities of the LMC disk. They conclude based upon these lines of evidence that the gas in these clouds is likely expelled from the LMC disk.

Our absorption line measurements are much more sensitive to low column density matter than the H I emission line measurements of Staveley-Smith et al. (2003). Thus, we are potentially probing gas with significantly different ionisation states. Indeed, Staveley-Smith et al. only display maps for the HVC material with N(H I) $\gtrsim 10^{18}$ cm^{-2}, which shows most of the gas concentrated to the southwestern edge of the LMC. Our lines of sight are concentrated significantly further to the east than most of their clouds. Danforth et al. (2002), however, have demonstrated that HVC material can be found over a substantial fraction of the LMC using *FUSE* absorption line measurements. Their measurements of Fe II equivalent widths towards LMC stars show a broad swath of high-velocity material covering the eastern edge of the galaxy, with the highest equivalent widths arising in the northeast quadrant. (Note that the coverage of the southwestern quadrant in their data was minimal.)

The most promising way to confirm our conclusion that the HVC material is associated with the LMC is to obtain absolute abundances of the HVC gas, which will require more sensitive H I emission line observations towards these sight lines. An absolute abundance derived from the ratio of O I to H I similar to the abundance of the LMC would strongly suggest an LMC origin.

While we acknowledge the uncertainties in this conclusion, we nonetheless proceed assuming that the HVC towards the LMC is associated with this galaxy. Thus, the velocity range for LMC gas along these sight lines should be defined as everything at $v_{\rm LSR} \gtrsim 100$ km s^{-1}. The velocities of the LMC IVC and HVC components indicate that they are expanding away from the warm disk gas or, for the gas at lower absolute velocities relative to the LMC disk, that the gas is extended above the disk, perhaps rotating in a thick disk. Only towards Sk-71°45 is there evidence for both significantly red-shifted and blue-shifted components in the weakly ionized species and O VI. Thus, little of the material we see can represent gas returning to the LMC disk. The velocity of the HVC relative to the LMC disk is larger than a simple estimate of the escape velocity of the LMC, $v_{esc} \approx \sqrt{2} v_{circ} \sim 100$ km s^{-1} (with $v_{circ} = 72 \pm 7$ km s^{-1} from Alves & Nelson 2000), implying that the material may escape the LMC, polluting the intergalactic space between the LMC and the Milky Way or serving as fuel for the Magellanic Stream.

The LMC-IVC may trace an interstellar thick disk about the LMC, perhaps similar to that seen about the Milky Way (e.g., Savage, Sembach, & Lu 1997). However, it seems unlikely that the HVC material can be associated with an extended, dynamically-supported thick disk component due to its extremely large velocity separation from the LMC. Theoretical modeling and stellar

observations of the LMC have revealed the existence of a stellar thick disk (e.g., Weinberg 2000; Bekki & Chiba 2005; Cole et al. 2005). Neither the simulations nor the observations of evolved stars demonstrate velocity dispersion greater than about 20–40 $\mathrm{km\,s^{-1}}$. While thick disk gas may not follow the stellar kinematics, it is unlikely that the velocity dispersion of the gas would be larger than that of stars since the gas is more subject to hydrodynamical effects than stars (i.e. gas is not collisionless). Gas corotating in a thickened disk may appear at lower velocities due to projection effects associated with the inclination of the LMC disk to our line of sight (see Howk et al. 2002). While this could contribute to the velocity shift of the LMC-IVC relative to the thin disk material, it does not produce a large enough velocity shift to explain the HVC velocities. Thus, the HVC material seems unlikely to be associated with a thick disk of material about the LMC. It is more likely tracing a large-scale outflow of material.

4.2.3 Physical origins

The comparison of the column densities of the highly ionised species can also be used to unravel their origins. The models summarized in Table 5 can be divided in 3 main mechanisms (Spitzer 1996): (i) conductive heating mechanisms (including the SNR, stellar winds, conductive interface, and shock ionisation) in which cool gas evaporates into adjacent hot medium (the highly ionised gas at $T \sim \mathrm{a\,few} \times 10^5$ being found at the interface between the cooler and hotter plasmas); (ii) radiative cooling models in which hot gas cools, (iii) the turbulent mixing layers where hot gas mixes with cool gas. The broad component of the highly ionised species therefore always probes indirectly the presence of hot gas ($T > 10^6$ K). In real physical environments, it is likely that these mechanisms are actually mixed all together to a certain degree, but depending on the physical conditions, one may dominate the other.

We discussed in the previous section that strong stellar winds (or SNRs) most certainly occur, at least in the bright H II and superbubble regions. Therefore some of the O VI and broad C IV and Si IV absorption must originate in the interface between the shocked plasma and the swept-up interstellar gas. In velocity space, most of this absorption should occur near the expanding shell velocity where part of the strong narrow components C IV and Si IV are observed. While the observed high-ion ratios are very roughly consistent with those models, the observations also suggest that the environments very local to our target stars have little discernible effect on the O VI/C IV ratios of the broad absorbing components. The O VI/C IV ratios are the highest towards the faint H II region associated with the supergiant shell DEM 48 (Sk$-65^\circ 22$) and towards the superbubble DEM 221 (Sk$-71^\circ 45$). They are the lowest towards the H II region DEM 241 (Sk$-67^\circ 211$) and the X-ray bright superbubble 30 Dor (Sk$-69^\circ 246$). This difference between the two superbubble sight lines and the two H II region sight lines makes it impossible to conclude that one type of structure is responsible for producing higher or lower O VI/C IV ratios. The absence of clear signature in the high-ion ratios may be because the individual clouds cannot be distinguished. A very large fraction of the observed O VI (and broad component of C IV and Si IV) must also have a different origin than the stellar environment itself (stellar wind and SNR models predict $N(\mathrm{O\ VI}) \sim \mathrm{a\,few} \times 10^{13}$ cm^{-2}, much less than the observed total O VI column density) and is not spatially localized near these H II regions and superbubbles even though some of it overlaps these structures in velocity space.

When the observed LMC-HVC high-ion ratios are compared to theoretical models (see Table 5), the turbulent mixing layer (TML) model always fails to produce large enough O VI/C IV; this is at odds with gas at the Milky Way velocities for which TMLs seem to be consistent with the observed ratios of highly ionised species (see Tables 4 and 5). One caveat to this conclusion is that if the oxygen abundance is systematically enhanced with respect to carbon, it would be likely that more O VI is observed than in "typical" regions in the Milky Way. But enhancement of oxygen or deficiency of carbon are not observed in the LMC (see Appendix in Welty et al. 1999, and references therein).

Another systematic between the various sightlines is deduced from Figs. 5 and 6 (see also discussion in §3): cooler gas traced by Si II and O I is observed at all velocities where O VI absorption is detected. The close correspondence in the total velocity extent of the observed Si II and O VI absorption strongly suggests that the high and the weakly ionised species are kinematically coupled. A correspondence between O VI and low-ion velocity extent has also been noted in the Milky Way (Howk, Savage, & Sembach 2003; Bowen et al. 2006). Such a relationship is expected if much or all of the O VI arises in interfaces between warm and hot gas. Borkowski, Balbus, & Fristrom (1990) present models of conductive interfaces in such an arrangement; they predict that if the O VI is found in both the evaporative and conductive stage, the O VI column density would be less than a few 10^{13} cm^{-2}, implying that each line of sight in our work intercepts 5–10 interfaces. The broadening of the high-ions is consistent with such an interpretation since, if there are 5–10 interfaces, each component of O VI could still have a temperature of a few times 10^5 K. While the low ion profiles are mostly unresolved, their velocity extents are consistent with a large number of components, and therefore with large number of interfaces. The profiles of weakly and highly ionised species cover a large enough velocity range that they are likely not simply tracing components associated directly with the H II regions or superbubbles housing the target stars. Thus, multiple interfaces are certainly possible and likely associated with gas out of the disk of the LMC. If conductive interfaces are the main origin for the broad component of the high ions, they have to be at least 3×10^5 year old to reproduce the high-ion ratios. We note that the observed O VI/Si IV ratios are somewhat smaller than the ratio predicted by Borkowski, Balbus, & Fristrom (1990), but Si IV can be easily photoionised by other sources (e.g., photons from stars or the absence of the incorporation of He II λ304 photons in the interface model that are capable of ionising efficiently Si III see Savage, Sembach, & Cardelli 1994), and this is not taken into account in their models. The limits derived from N V are always consistent with the conductive interface models. It is not clear within the frame work of the conductive interface models why the high-ion ratios would be similar over the large velocity range between the LMC and HVC components, and yet so dissimilar between the observed sightlines.

In view of the complexity of the profiles and of the physical regions probed, other models may be in play, especially in the event that the apparent kinematic coupling does not imply coincidence of the highly and weakly ionised gas:

– Strong shocks with $v_{\mathrm{shock}} > 200\ \mathrm{km\,s^{-1}}$ would produce enough O VI to explain the observed ratios. Such strong shocks have not been inferred in the denser parts of H II and superbubble regions of the LMC (Oey et al. 2000). But high-velocity shocks are likely to arise in low-density gas where they remain undected since they would not contribute to the nebular emission (Y.-H. Chu 2006, priv. comm.). The strong shock models are attractive because they provide a straightforward method for producing a consistent O VI/C IV ratio over a large range of velocities. If such strong shocks occur in the LMC, the gas traced by the LMC-IVC/HVC

Table 7. Interstellar O VI and environments in the LMC

Id.	Star	R.A. (°)	Dec. (°)	$\log N$(O VI) (dex)	Environments
1	Sk−67°05	72.58	–67.66	13.89 ± 0.07	H II region DEM 7
2	Sk−67°20	73.88	–67.50	14.26 ± 0.10	Field star, no Hα
3	Sk−65°22	75.34	–65.87	14.14 ± 0.02	Supergiant shell DEM 48
4	Sk−66°51	75.79	–66.68	14.31 ± 0.07	H II region DEM 56, no Hα
5	Sk−67°69	78.58	–67.13	14.48 ± 0.03	H II region DEM 107
6	Sk−68°80	81.62	–68.84	14.61 ± 0.04	X-ray bright superbubble DEM 199
7	Sk−70°91	81.89	–70.61	14.55 ± 0.07	Superbubble DEM 208
8	Sk−66°100	81.94	–66.92	14.26 ± 0.06	Field star, no Hα
9	Sk−67°144	82.55	–67.43	14.41 ± 0.07	Periphery of supergiant shell LMC 4
10	Sk−71°45	82.81	–71.06	14.37 ± 0.02	Superbubble DEM 221
11	Sk−69°191	83.58	–69.75	14.38 ± 0.06	X-ray bright superbubble DEM 246
12	Sk−67°211	83.80	–67.55	14.20 ± 0.02	H II region DEM 241
13	BI 237	84.06	–67.65	14.39 ± 0.03	Diffuse H II region
14	Sk−66°172	84.27	–66.35	14.31 ± 0.06	H II region DEM 252
15	Sk−69°246	84.72	–69.03	14.36 ± 0.08	X-ray bright superbubble 30 Dor
16	<N 70>	85.81	–67.85	14.48 ± 0.10	Superbubble DEM 301
17	CAL 83	85.89	–68.37	14.39 ± 0.08	Field star
18	BI 272	86.09	–67.24	14.30 ± 0.03	Diffuse H II region DEM 309
19	Sk−67°266	86.46	–67.24	14.09 ± 0.07	Shell DEM 315

Note: O VI column densities are from this work, Howk et al. (2002), and Danforth & Blair (2006). The designations DEM refer to entry in the catalog of Davies, Elliott, & Meaburn (1976).

components could have been ejected away from the LMC in this process.

– The non-equilibrium radiative cooling model of Edgar & Chevalier (1986) where a gas cools from temperature of $\gtrsim 10^6$ K fits also the data when O VI/C IV is greater than 5.9. More recently, Gnat & Sternberg (2006) have produced new calculations of radiatively cooling gas as a function of metallicity using updated atomic data. The O VI/C IV and O VI/Si IV ratios for the HVC and LMC absorbers are consistent with the Gnat & Sternberg models of radiative cooling from $T \sim 5 \times 10^6$ K for models with metallicities 0.1 to 1.0 times solar. The gas must still be at temperatures between $\sim (1-2) \times 10^5$ K in order to match their models. A radiative cooling model for the origins of the highly-ionised gas in the HVC and LMC components would be consistent with an outflow and infall of highly ionised material from the disk of the LMC, i.e., an exchange of matter between the thin disk of the LMC and its halo or thick disk. The majority of the gas must cool in the outflow phase since we only find evidence for the possible infall of material towards one sight line. If we combine our sample with that of Howk et al. (2002), only 3 of 14 sight lines show possible evidence for infalling material. It is, however, not clear within the framework of this model why velocities of the cool and hotter gas would be systematically coincident.

In summary, the physical origins of O VI and broad C IV and Si IV are tangled and several processes could occur. However, it is apparent that conducting heating processes play a fundamental role in the production of the highly ionised species probing gas at $T \sim 10^5$ K while TMLs are not important in the probed regions in the HVC-LMC, except if a large fraction of O VI is produced via another mechanism (e.g., radiative cooling).

4.2.4 Fluctuation of N(O VI)

We note that Danforth & Blair (2006) found that the O VI column densities appear higher by about 0.2 dex in the N 70 superbubble and other superbubbles described by Howk et al. (2002) compared to some more quiescent H II region sight lines, suggesting the very local environment of the background stars may affect the total column of O VI along a sight line. In this context, they argued that superbubbles were significant contributors to the total O VI observed along LMC sight lines. Fig. 8 shows an Hα image of the LMC from Gaustad et al. (2001) with a representation of all available O VI column densities superimposed (including Danforth & Blair 2006; Howk et al. 2002, and this work). Table 7 summarises the measured columns and the surrounding environments for each *FUSE* measurement. All of the superbubble sight lines are concentrated below the line superimposed on the image (we display only the average of the four measurements towards N70).

While some superbubble-type regions may have slight enhancements in O VI, what is striking about this figure is the very large local variations, as reported by Howk et al. (2002). For example the pairs of stars labeled 12 & 13 (Sk−67°211 & BI 237) and 18 & 19 (BI 272 and Sk−67°266) trace H II regions where the column densities varies by a factor 2 from 14.1 to 14.4 dex. These pairs have projected separations of 90 and 129 pc, respectively. This is the degree of enhancement Danforth & Blair (2006) identify with superbubbles, but over much smaller angular scales than those authors use for comparison between superbubble and non-superbubble sight lines. Furthermore quiescent regions like stars no. 2, 5, and 17 have O VI column densities similar or larger than observed in some superbubbles. The dispersion of N(O VI) is large along superbubble sight lines, as well. The measurements of N(O VI) appear not to be smaller than 14.3 dex in the superbubbles. However, many more O VI measurements will be needed in the LMC before one can truly determine if the superbubbles and other very local phenomena have a strong impact on the observed total O VI column density. It is clear that the O VI has a patchy distribution in the LMC, and comparisons between sight lines separated by tens of parsecs may not lead to significant results in this regard. While the high-ion ratios vary from sight line to sight line, there is no clear link between the observed variation and the regions associated with the lines of sight. The comparison of high-ion ratios

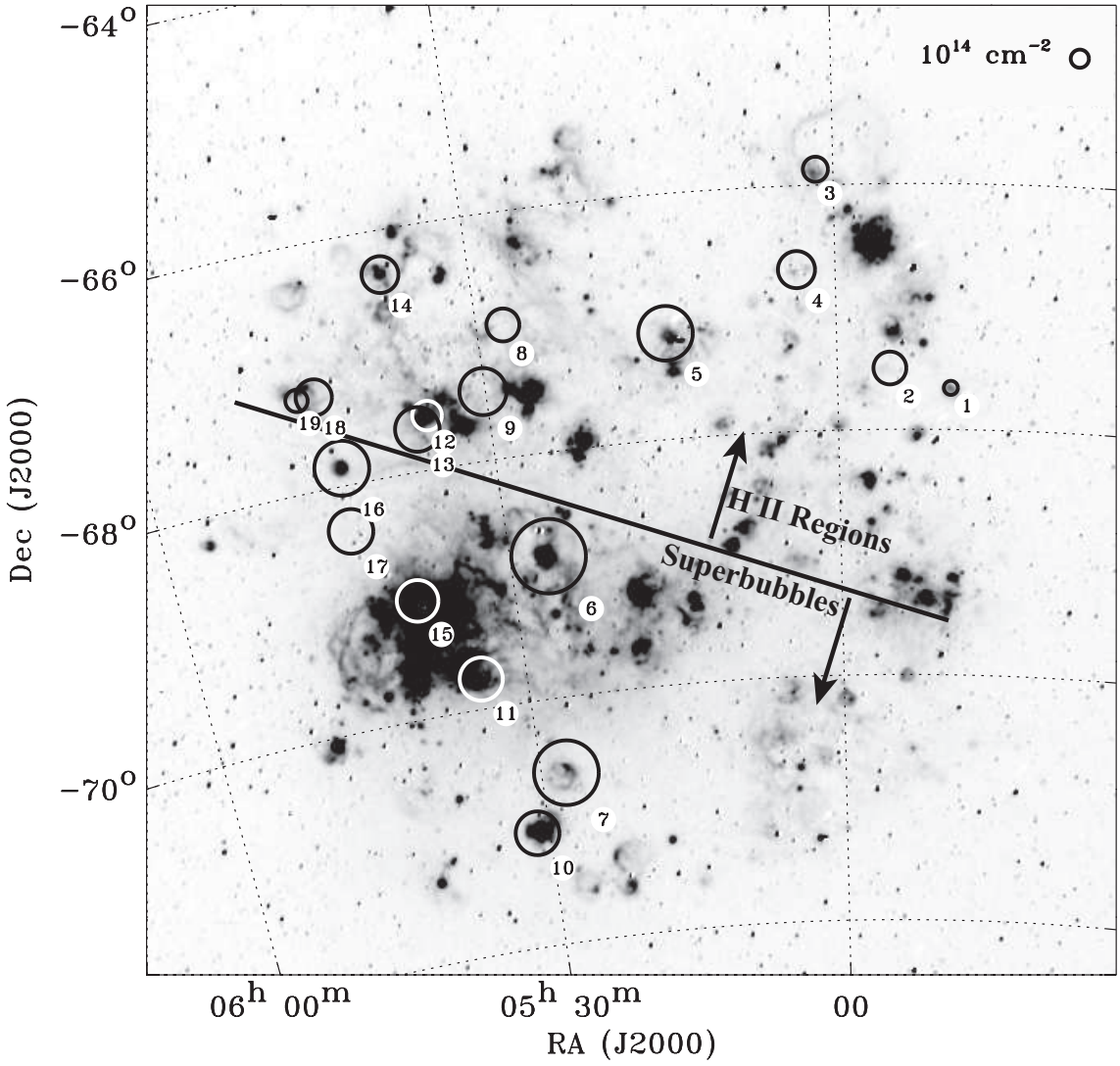

Figure 8. Hα image of the LMC (Gaustad et al. 2001). The identification numbers are summarised in Table 7. Darker regions correspond to brighter Hα emission. The radius of the circle marking each probe star is linearly proportional to the column density of interstellar O VI at LMC velocities. *Note that the apparent emission near no. 5 is caused by an imperfectly subtracted foreground star*. Fortuitously, the superbubbles are well separated from the H II regions (except for no. 17, which is an H II region) and the solid line marks the separation between them. Note that several H II regions are associated with supergiant shells.

is potentially a more secure indicator of the impact of the local effects because it is not subject to the varying depth of the gas probed by the background stars, which may be part of the source of the observed variations in N(O VI).

5 SUMMARY

We analyse the physical properties of the highly ionised species (C IV, Si IV, N V, O VI) in and around the LMC towards a sample of 4 LMC hot stars. Two of these sight lines probe prominent superbubbles, while the other two probe H II regions, allowing us to compare the highly ionised species and their connection with weakly ionised species among different regions. O VI was obtained with *FUSE* with a spectral resolution of $\sim$20 km s^{-1}, and the other highly ionised species were observed with the *HST*/STIS E140M setup with a spectral resolution of $\sim$7 km s^{-1}. The excellent spectral resolution and high signal-to-noise of these data have allowed us to model the highly ionised species in the LMC. Our main findings are summarised as follows:

(i) Absorption from both the high and low ionisation species are observed over the entire range of velocities from the Milky Way to LMC ($-50 \lesssim v_{\rm LSR} \lesssim +350$ km s^{-1}). Along our four sight lines, the profiles are separated into four principal components: the MW ($v_{\rm LSR} \lesssim 30$ km s^{-1}), IVC ($30 \lesssim v_{\rm LSR} \lesssim 100$ km s^{-1}), HVC ($100 \lesssim v_{\rm LSR} \lesssim 175$ km s^{-1}), and LMC ($v_{\rm LSR} \gtrsim 175$ km s^{-1}). N V is not detected at the 3σ level.

(ii) In the LMC component, we find narrow and broad absorption in C IV and Si IV, but only very broad O VI absorption. The narrow LMC components of C IV and Si IV have an observed b-value that implies temperatures of a few times 10^4 K or less. The properties of the narrow components of C IV and Si IV can be principally explained by the interstellar environment associated with the stars, in particular H II regions around the central star and expanding shells behind the shocked plasma.

(iii) The O VI at LMC velocities is broader than the O VI

absorption observed in the combined Milky Way and IVC component, implying that the LMC O VI profiles are composed of several components. The broad LMC components of O VI, C IV, and Si IV likely probe gas of a few times 10^5 K.

(iv) We find a striking similarity in the O VI/C IV ratios for the LMC and HVC components ($v_{\rm LSR} \gtrsim 100$ km s^{-1}) along a given sight line, but the O VI/C IV ratios for the HVC and LMC gas vary between the sight lines (see Fig. 7). The fact that the ratios in the HVC and LMC components along a given sight line are always very similar suggests that the HVC component has its origins in the LMC, and the processes producing the highly-ionised gas in the LMC affect a large range of velocities along a given sight line.

(v) The difference in the high-ion ratios between the four sight lines implies different processes or varying conditions may produce the highly ionised species in the LMC. There is no evidence, however, of a link between the observed variation and the regions associated with the stars, although it is likely that some of the O VI absorption occurs because of stellar winds or other phenomena associated with the stellar environment. Conductive interface model can reproduce both the high-ion ratios observed in the broad component and the apparent kinematically coupling between O VI and the weakly ionised species such as Si II and O I.

(vi) The velocities of the LMC-IVC and HVC components indicate that they are expanding away from the warm disk gas. Only towards one line of sight is there evidence for both significant redshifted and blue-shifted components in the low- and high-ion spectra, implying little of the material we observe is returning to the LMC disk. Our analysis therefore provides compelling evidence for a hot LMC halo fed by energetic outflows from the LMC disk and even possibly with a galactic wind since the velocity of the HVC relative to the LMC disk is actually large enough to escape the LMC.

ACKNOWLEDGEMENTS

We are grateful to You-Hua Chu and Blair Savage for useful comments on an earlier draft. We also thank You-Hua Chu for sharing unpublished Hα velocities. We recognise partial support by the National Science Foundation grant AST 06-07731 and appreciate support from the University of Notre Dame. Based on observations made with the NASA-CNES-CSA Far Ultraviolet Spectroscopic Explorer. FUSE is operated for NASA by the Johns Hopkins University under NASA contract NAS5-32985. Based on observations made with the NASA/ESA Hubble Space Telescope, obtained at the Space Telescope Science Institute, which is operated by the Association of Universities for Research in Astronomy, Inc. under NASA contract No. NAS5-26555. This research has made use of the NASA Astrophysics Data System Abstract Service and the SIMBAD database, operated at CDS, Strasbourg, France.

REFERENCES

Abbott D. C., 1982, ApJ, 263, 723
Alves, D. R., & Nelson, C. A., 2000, ApJ, 542, 789
Bekki K., Chiba M., 2005, MNRAS, 356, 680
Black, J.H., Dupree, A.K., Hartmann, L.W., Raymond, J.C. 1980, ApJ, 239, 502
Boehringer H., Hartquist T. W., 1987, MNRAS, 228, 915
de Boer K. S., Savage B. D., 1980, ApJ, 238, 86
Borkowski K. J., Balbus S. A., Fristrom C. C., 1990, ApJ, 355, 501
Bowen, D. V., Jenkins, E. B., Tripp, T. M., Sembach, K. R., Savage, B. D., 2006, in "Astrophysics in the Far Ultraviolet: Five Years of Discovery with FUSE", Eds. G. Sonneborn, H. Moos, and B.-G. Andersson, p. 412
Breitschwerdt D., Voelk H. J., McKenzie J. F., 1991, A&A, 245, 79
Castor J., McCray R., Weaver R., 1975, ApJ, 200, L107
Chu Y.-H., Guerrero M. A., Gruendl R. A., 2004, hdgw.conf, 165
Chu Y.-H., Kennicutt R. C., Jr., 1994, ApJ, 425, 720
Chu Y.-H., Wakker B., Mac Low M.-M., Garcia-Segura G., 1994, AJ, 108, 1696
Cole A. A., Tolstoy E., Gallagher J. S., III, Smecker-Hane T. A., 2005, AJ, 129, 1465
Cowie, L.L., Taylor, W., York, D.G. 1981, ApJ, 248, 528
Danforth C. W., 2003, PhD Thesis
Danforth C. W., Blair W. P., 2006, ApJ, 646, 205
Danforth C. W., Howk J. C., Fullerton A. W., Blair W. P., Sembach K. R., 2002, ApJS, 139, 81
Davies R. D., Elliott K. H., Meaburn J., 1976, MNRAS, 81, 89
Dopita M. A., Sutherland R. S., 1996, ApJS, 102, 161
Dupree A. K., Raymond J. C., 1983, ApJ, 275, L71
Edgar, R. J., Chevalier, R. A. 1986, ApJ, 310, L27
Ferland, G.J., et al. 1998, PASP, 110, 761
Fitzpatrick, E.L., Spitzer, L. 1997, ApJ, 475, 623
Fox A. J., Savage B. D., Sembach K. R., Fabian D., Richter P., Meyer D. M., Lauroesch J., Howk J. C., 2003, ApJ, 582, 793
Fox A. J., Wakker B. P., Savage B. D., Tripp T. M., Sembach K. R., Bland-Hawthorn J., 2005, ApJ, 630, 332
Gnat, O., Sternberg, A., 2006, ApJS, in press (astro-ph/0608181)
Gaustad, J.E., McCullough, P.R., Rosing, W., Van Buren, D. 2001, PASP, 113, 1326
Henize K. G., 1956, ApJS, 2, 315
Hoopes, C. G., Sembach, K. R., Howk, J. C., Savage, B. D., Fullerton, A. W. 2002, ApJ, 569, 233
Howk, J. C., Savage, B. D., Sembach, K. R., 2003, ApJ, 586, 249
Howk, J. C., Sembach, K. R., Savage, B. D., Massa, D., Friedman, S. D., Fullerton, A. W. 2002, ApJ, 569, 214
Indebetouw R., Shull J. M., 2004, ApJ, 605, 205
Kafatos M., 1973, ApJ, 182, 433
Knauth D. C., Howk J. C., Sembach K. R., Lauroesch J. T., Meyer D. M., 2003, ApJ, 592, 964
Lehner, N., Fullerton, A. W., Sembach, K. R., Massa, D. L., Jenkins, E. B. 2001, ApJ, 556, L103
Mac Low M.-M., McCray R., 1988, ApJ, 324, 776
Massa D., Fullerton A. W., Sonneborn G., Hutchings J. B., 2003, ApJ, 586, 996
Matteucci F., 2003, Ap&SS, 284, 539
Meaburn J., 1980, MNRAS, 192, 365
Moos, H. W. et al. 2000, ApJ, 538, L1
Morton, D. C. 2003, ApJS, 149, 205
Norman C. A., Ikeuchi S., 1989, ApJ, 345, 372
Oey M. S., Dopita M. A., Shields J. C., Smith R. C., 2000, ApJS, 128, 511
Oey M. S., García-Segura G., 2004, ApJ, 613, 302
Recchi S., Matteucci F., D'Ercole A., 2001, MNRAS, 322, 800
Russell, S.C., & Dopita, M.A. 1992, ApJ, 384, 508
Sahnow, D. S. et al. 2000, ApJ, 538, L7
Savage, B. D., Lehner, N. 2006, ApJS, 162, 134
Savage B. D., Sembach K. R., Cardelli J. A., 1994, ApJ, 420, 183
Savage B. D., Sembach K. R., Lu L., 1997, AJ, 113, 2158

Savage, B. et al. 2003, ApJS, 146, 125
Savage, B. D., Sembach, K. R. 1991, ApJ, 379, 245
Sembach K. R., 1994, ApJ, 434, 244
Sembach, K. R., Savage, B. D. 1992, ApJS, 83, 147
Sembach, K. R. et al. 2003, ApJS, 146, 165
Shapiro P. R., Field G. B., 1976, ApJ, 205, 762
Shapiro P. R., Moore R. T., 1976, ApJ, 207, 460
Shelton R. L., 1998, ApJ, 504, 785
Shull J. M., Slavin J. D., 1994, ApJ, 427, 784
Slavin, J. D. 1989, ApJ, 346, 718
Slavin J. D., Cox D. P., 1992, ApJ, 392, 131
Slavin, J. D., Cox, D. P. 1993, ApJ, 417, 187
Slavin J. D., Shull J. M., Begelman M. C., 1993, ApJ, 407, 83
Spitzer, L. J. 1996, ApJ, 458, L29
Staveley-Smith L., Kim S., Calabretta M. R., Haynes R. F., Kesteven M. J., 2003, MNRAS, 339, 87
Sutherland, R. S., Dopita, M. A. 1993, ApJS, 88, 253
Tomisaka K., Ikeuchi S., 1986, PASJ, 38, 697
Townsley L. K., Broos P. S., Feigelson E. D., Garmire G. P., Getman K. V., 2006, AJ, 131, 2164
Wakker B., Howk J. C., Chu Y.-H., Bomans D., Points S. D., 1998, ApJ, 499, L87
Wakker, B. P. et al. 2003, ApJS, 146, 1
Walborn N. R., Fullerton A. W., Crowther P. A., Bianchi L., Hutchings J. B., Pellerin A., Sonneborn G., Willis A. J., 2002, ApJS, 141, 443
Weaver R., McCray R., Castor J., Shapiro P., Moore R., 1977, ApJ, 218, 377
Welty D. E., Hobbs L. M., Lauroesch J. T., Morton D. C., Spitzer L., York D. G., 1999, ApJS, 124, 465
Weinberg M. D., 2000, ApJ, 532, 922
Willis A. J., Crowther P. A., Fullerton A. W., Hutchings J. B., Sonneborn G., Brownsberger K., Massa D. L., Walborn N. R., 2004, ApJS, 154, 651
Zsargó, J., Sembach, K. R., Howk, J. C., Savage, B. D. 2003, ApJ, 586, 1019

This paper has been typeset from a TEX/ LATEX file prepared by the author.